The Astrophysical Journal Supplement Series, 165:461–479, 2006 August

HIGH-RESOLUTION OPTICAL VELOCITY FIELDS OF 11 LOW SURFACE BRIGHTNESS GALAXIES

Rachel Kuzio de Naray[1] and Stacy S. McGaugh[1]
Department of Astronomy, University of Maryland, College Park, MD 20742-2421; kuzio@astro.umd.edu, ssm@astro.umd.edu
W. J. G. de Blok[1]
Research School of Astronomy and Astrophysics, Mount Stromlo Observatory, Cotter Road, Weston Creek, ACT 2611, Australia; edeblok@mso.anu.edu.au
and
A. Bosma
Observatoire de Marseille, 2 Place Le Verrier, 13248 Marseille Cedex 4, France; bosma@oamp.fr
Received 2005 December 13; accepted 2006 April 24

ABSTRACT

We present high-resolution two-dimensional velocity fields from integral field spectroscopy, along with derived rotation curves for 11 low surface brightness galaxies. We fit NFW and pseudoisothermal halo models to the new data combined with previous long-slit and H I data. In most cases, we find the pseudoisothermal halo to better represent the data than the NFW halo, as the NFW concentrations are often lower than expected for a ΛCDM cosmology. We also compare our results to previous studies and find that including the new two-dimensional optical data does not significantly alter the halo parameters but does decrease the uncertainties by roughly a factor of 2.

Subject headings: dark matter — galaxies: fundamental parameters — galaxies: kinematics and dynamics

Online material: color figures

1. INTRODUCTION

Determining the mass density profiles of galactic dark matter halos has been an exciting, yet contentious, field for a number of years now. Although it is widely agreed that low surface brightness (LSB) galaxies are dark matter–dominated down to small radii (de Blok & McGaugh 1996, 1997; Pickering et al. 1997, 1999; Blais-Ouellette et al. 2001; Borriello & Salucci 2001; Simon et al. 2003; but see Fuchs 2003) and, hence, are ideal test subjects for studying the dark matter distribution, a consensus on the interpretation of their rotation curves has been difficult to achieve.

The disagreement arises when comparing the data to numerical simulations of cold dark matter (CDM). The most common description of CDM halo behavior is given by the analytic approximation of Navarro et al. (1996, 1997) and is known as the NFW profile. The cosmologically motivated NFW halo is characterized by a mass density that rises very steeply toward the center, a property that makes the halo "cuspy." Cuspy halos that rise more steeply than the NFW halo have also been suggested (e.g., Moore et al. 1999; Reed et al. 2003; Navarro et al. 2004; Diemand et al. 2005). Whether or not the dark matter halos of LSB galaxies can be described by cuspy NFW-like profiles has been a matter of debate.

NFW halos can be fitted to the observations, but the fits are usually of lower quality than fits with pseudoisothermal halos. Moreover, the implied cosmological parameters are inconsistent with the standard ΛCDM picture. In particular, the observed concentrations of the NFW halos are too low (McGaugh et al. 2003; Swaters et al. 2003b). Much better fits to LSB observations are found when using the pseudoisothermal halo model (Simon et al. 2005; de Blok et al. 2001a, 2001b [hereafter BMR01], 2003; de Blok & Bosma 2002 [hereafter BB02]; Marchesini et al. 2002; Bolatto et al. 2002; Blais-Ouellette et al. 2001; Côté et al. 2000). These halos have a mass density that remains at an approximately constant value toward the center; thus, they are referred to as "cored" halos. Unlike the NFW profile, however, the pseudoisothermal halo has no cosmological motivation or theoretical basis.

In its favor, the CDM model has been successful on large scales in explaining structure formation in the early universe, as well as abundances of galaxy clusters (Tegmark et al. 2004). It is more appealing to have a halo model with explanations rooted in cosmology than a model that is simply a convenient fit to the data. It is therefore no surprise that a number of reasons have been given in an attempt to salvage the appropriateness of the NFW profile as a description of galactic dark matter halos.

The earliest observations that indicated cores in LSB galaxies were two-dimensional 21 cm H I velocity fields (Moore 1994; Flores & Primack 1994; de Blok et al. 1996 [hereafter BMH96]). Low spatial resolution (i.e., beam smearing) was suggested to be a systematic effect that would erroneously indicate cores (van den Bosch et al. 2000; Swaters et al. 2000). The question of beam smearing was addressed by long-slit Hα observations, which had an order-of-magnitude increase in spatial resolution (see, e.g., McGaugh et al. 2001 [hereafter MRB01]; BMR01); cusps did not appear when the resolution was increased, showing that beam smearing had been of only minor importance in the H I observations. Possible systematic errors in the long-slit spectroscopy (e.g., Simon et al. 2003; Rhee et al. 2004; Spekkens et al. 2005) have since become the focus of attention, with slit misplacement (Swaters et al. 2003a) and noncircular motions among the top concerns. If the slit misses the dynamical center of the galaxy or if there are noncircular motions from, for instance, a bar, the circular velocity may be underestimated and lead to the false inference of a cored halo. De Blok et al. (2003) conducted extensive modeling in which the rotation curves of both cuspy and cored halos were subjected to various effects and concluded that

[1] Visiting Astronomer, Kitt Peak National Observatory, National Optical Astronomy Observatory, which is operated by the Association of Universities for Research in Astronomy (AURA), Inc., under cooperative agreement with the National Science Foundation.

no systematic effect will entirely mask the presence of a cuspy halo for realistic observing conditions. Swaters et al. (2003a) performed a similar exercise with similar results but argued that it might still be possible to retain cuspy halos.

Clearly, there are a number of issues that new observations must simultaneously address. The data must be both high-resolution and two-dimensional in nature. Observations must have resolution $\lesssim$1 kpc, as that is the critical length scale at which the distinction between cusps and cores can be determined (de Blok 2004). Any noncircular motions should be readily identifiable in a two-dimensional velocity field. In addition, slit placement is not a concern of two-dimensional velocity fields. This observational approach has also been applied by such groups as Simon et al. (2003, 2005).

In this paper, we present the rotation curves derived from high-resolution two-dimensional velocity fields of a sample of LSB galaxies. In § 2, we discuss the sample and observations; data reduction is discussed in § 3. The results for the individual galaxies are presented in § 4. In § 5, we discuss halo fits to the minimum-disk case of the new data combined with previous long-slit and H I rotation curves and compare our results to those of previous studies. Noncircular motions are also briefly discussed. Our conclusions and goals for future work are stated in § 6.

2. SAMPLE AND OBSERVATIONS

Our primary targets were the galaxies in the "clean" sample of de Blok et al. (2003). In brief, galaxies in the "clean" sample have inclinations between 30° and 85°, are likely to meet the minimum-disk assumption, have long-slit rotation curves that are well resolved in the inner 1 kpc, have small error bars, and lack large asymmetries. The minimum-disk assumption is considered applicable to those galaxies that require substantial amounts of dark matter at small radii even in the maximum-disk model. We then expanded our sample to include other LSB galaxies that nearly made the "clean" cut. We also searched for low-mass dwarf galaxies to fill out the range of right ascension available at the telescope, giving preference to those targets with diffuse Hα emission detected by long-slit observations.

We observed eight "clean" galaxies: UGC 4325, DDO 64, NGC 4395, F583-4, F583-1, DDO 185, DDO 189, and NGC 4455. These galaxies were selected from the "clean" sample because the well-resolved long-slit Hα observations (BB02; BMR01) show that there is diffuse Hα emission for detectability in two-dimensional velocity fields and that the galaxies lack indicators of significant noncircular motions (e.g., strong bars or gross asymmetries). While not a criterion considered in the selection process, it turns out that the long-slit observations of these galaxies imply that the galaxies either have unreasonably low NFW concentrations or do not have cusps at all. These kinds of galaxies pose the biggest problem for CDM and, as such, provide important test cases.

We observed four galaxies from MRB01 (F563-V2, F563-1, F568-3, and UGC 5750) that almost made the "clean" sample. They show diffuse Hα emission but either did not have the required number of independent points in the inner 1 kpc of the long-slit rotation curve or had an inclination outside the "clean" range.

Finally, we observed 16 galaxies from the Nearby Galaxies Catalogue (Tully 1988). Selection criteria for these galaxies included positions satisfying $18^{\rm h} \lesssim \alpha \lesssim 08^{\rm h}$ and $+10^\circ \lesssim \delta \lesssim +50^\circ$, inclinations between 30° and 85°, heliocentric velocities $\lesssim$2500 km s^{-1}, and an estimated $V_{\rm flat}$ (approximated by $V_{\rm flat} \sim 0.5 W_{20} \sin^{-1} i$) between roughly 50 and 100 km s^{-1}.

Our sample of 28 observed galaxies is both weather- and signal-limited. Poor weather prevented us from observing more of the "clean" sample. Our sample is signal-limited in that not all of the galaxies have enough Hα emission to construct useful velocity fields. While preexisting long-slit observations can be used as a guide, there is no way of knowing how much Hα emission will be detected by the integrated field unit (IFU) until the experiment is done. Our sample is intentionally focused on the most dark matter–dominated objects. These tend to be very low surface brightness dwarfs that are hard to observe.

The galaxies were observed during the nights of 2004 April 12–15, 2004 November 14–19, and 2005 September 1–7. Observations were made using the DensePak IFU on the 3.5 m WIYN[2] telescope at the Kitt Peak National Observatory (KPNO). DensePak is comprised of 3″ diameter fibers arranged in a 43″ × 28″ rectangle. We measured the fiber separation to be 3.″84. The separation was determined by centering a bright star in a fiber and repeatedly shifting between fibers and across the array. There are 85 working fibers in this arrangement; an additional four sky fibers are arranged outside the main bundle. We used the 860 lines mm^{-1} grating in second order, centered near Hα, giving a 58 km s^{-1} velocity resolution. The distances to the galaxies in the sample are such that a 3″ fiber provides subkiloparsec resolution.

Because the galaxies were too faint to be visible on the guide camera, we centered the DensePak array on a nearby star and then offset to the optical center of the galaxy. Subsequent pointings on the galaxy were made by shifting the array by small amounts from its current position. For a number of galaxies, these moves were the fine shifts required to observe the spaces between the fibers. These interstitial pointings effectively increased the resolution to ~2″. The fiber bundle orientation on the sky and the total number of pointings per galaxy were tailored to each galaxy so that the critical central regions were covered by the DensePak fibers. Each exposure was 1800 s, and two exposures were taken at each pointing. A CuAr lamp was observed before and after each pointing to provide wavelength calibration.

3. DATA REDUCTION

The observations were reduced in IRAF[3] using the HYDRA package. The data were bias-subtracted and flattened. The IRAF task `dohydra` was used to extract the spectra. A wavelength solution created from the observations of the CuAr lamp was applied to the spectra. The two exposures per pointing were combined to increase the signal-to-noise ratio and to remove cosmic rays. Sky subtraction was not performed, because the DensePak sky fibers often fell inside the galaxies rather than on the sky and were therefore contaminated by galactic emission. We made use of the night-sky emission lines by using them as the reference wavelengths (Osterbrock et al. 1996) by which the velocities of the galactic emission lines were measured. We also tried using the CuAr calibration to measure the velocities, but the night-sky lines gave cleaner results. Velocities were measured by fitting Gaussians to both the sky lines and the four galactic emission lines of interest: Hα, [N II] λ6584, [S II] λ6717, and [S II] λ6731. The average error on individual emission-line velocities due to centroiding accuracy was roughly 1.5 km s^{-1}. We used the arithmetic mean of the

[2] Based on observations obtained at the WIYN Observatory. The WIYN Observatory is a joint facility of the University of Wisconsin–Madison, Indiana University, Yale University, and the National Optical Astronomy Observatory.

[3] IRAF is distributed by the National Optical Astronomy Observatory, which is operated by the Association of Universities for Research in Astronomy (AURA), Inc., under agreement with the National Science Foundation.

TABLE 1
PROPERTIES OF OBSERVED GALAXIES

Galaxy (1)	R.A. (J2000.0) (2)	Decl. (J2000.0) (3)	$\mu_0(R)$ (mag arcsec^{-2}) (4)	Distance (Mpc) (5)	i (deg) (6)	V_{hel} (km s^{-1}) (7)	R_{max} (kpc) (8)	V_{max} (km s^{-1}) (9)	P.A. (deg) (10)	References (11)
UGC 4325	08 19 20.5	+50 00 35	21.6	10.1	41	514	2.3	86	52	1
F563-V2	08 53 03.7	+18 26 09	21.2[a]	61	29	4316	6.7	104	328	2
F563-1	08 55 06.9	+19 44 58	22.6	45	25	3482	5.6	146	341	2
DDO 64[b]	09 50 22.4	+31 29 16	...	6.1	60	520	2.1	51	97	1
F568-3	10 27 20.3	+22 14 22	22.2[a]	77	40	5905	8.4	114	169	2
UGC 5750	10 35 45.1	+20 59 24	22.6	56	64	4160	8.5	61	167	1
NGC 4395[c]	12 25 48.9	+33 32 48	22.2	3.5	46	310	0.8	33	327	1
F583-4	15 52 12.7	+18 47 06	22.9[a]	49	55	3620	7.5	75	115	2
F583-1	15 57 27.5	+20 39 58	23.2[a]	32	63	2256	4.9	83	355	2
UGC 477	00 46 13.1	+19 29 24	...	35	82	2635	10	112	347	3
UGC 1281	01 49 32.0	+32 35 23	22.7[d]	5.5	85	145	1.9	38	218	3

NOTES.—Units of right ascension are hours, minutes, and seconds, and units of declination are degrees, arcminutes, and arcseconds. Col. (1): Galaxy name. Col. (2): Right ascension. Col. (3): Declination. Col. (4): Central surface brightness in R-band. Col. (5): Distance. Col. (6): Inclination. Col. (7): Heliocentric systemic velocity. Col. (8): Maximum radius of the DensePak rotation curve. Col. (9): Maximum velocity of the DensePak rotation curve. Col. (10): Position angle of major axis; see § 4 for details. Col. (11): References for surface brightness, distance, and inclination.

[a] Converted from B band assuming $B - R = 0.9$.

[b] DDO 64 = UGC 5272.

[c] NGC 4395 = UGC 7524.

[d] Taken from BB02.

REFERENCES.—(1) BB02; (2) BMR01; (3) Tully 1988.

measured emission-line velocities in each fiber as the fiber velocity. The maximum difference between the measured velocities and the mean was taken to be the error on the fiber velocity. Many of these errors were less than 5 km s^{-1}, although a few were as high as ~20 km s^{-1}. If only Hα was observed in a fiber, the observed Hα velocity was taken as the fiber velocity and the error was set to 10 km s^{-1}.

The observed velocity fields were made by combining the individual DensePak pointings using the input shifts at the telescope. To confirm the accuracy of the offsets, an Hα flux image of the galaxy constructed from the DensePak observations was compared to an actual Hα image. Relative positions between features in the galaxy (i.e., bright H II regions) in the two images were measured and compared. The fluxes in any overlapping fibers were also compared. The accuracy of the fiber positions is ~0.″6, and we found the telescope to be capable of accurately shifting from the nearby bright offset stars (typically 1′–2′ shifts), as well as the smaller distances (~0.″7 shifts) required to observe the spaces between the DensePak fibers. The telescope pointing is robust and repeatable.

We used the NEMO (Teuben 1995) program ROTCUR (Begeman 1989) to derive rotation curves from our two-dimensional data. ROTCUR treats the observed velocity field as an ensemble of tilted rings and then fits for the center, systemic velocity, inclination, position angle, and rotation velocity in each ring. Specifically, ROTCUR does a nonlinear least-squares fit to the following equation:

$$V(x, y) = V_{sys} + V_{rot} \cos\theta \sin i, \quad (1)$$

where

$$\cos\theta = \frac{-(x - x_0)\sin(\mathrm{PA}) + (y - y_0)\cos(\mathrm{PA})}{r} \quad (2)$$

and

$$r^2 = (x - x_0)^2 + (y - y_0)^2/\cos^2 i. \quad (3)$$

The observed velocity at position x, y, $V(x, y)$, is a function of the systemic velocity (V_{sys}), the rotation velocity (V_{rot}), the inclination (i), the position of the center of rotation (x_0, y_0), and the position angle (PA) of the major axis. The position angle is defined as the angle between north and the receding side of the major axis, measured from north through east. Each point is weighted by the inverse square of the error on the fiber velocity times $\cos(\theta)$, the angle away from the major axis.

The DensePak data cover the centers of the galaxies. We find these to be in the regime of solid-body rotation. Consequently, neither the center nor the inclination could be determined by the observations. The center was therefore fixed to the position of the optical center, and the inclination was fixed to published values (BMR01; BB02; Tully 1988). The systemic velocities were determined by ROTCUR. We also used ROTCUR to determine the position angle of the major axis, using published long-slit values as the initial guess. If the position angle could not be well constrained by ROTCUR, then it was fixed to the long-slit value. The long-slit position angles are generally from either the H I velocity field or the surface photometry, or, in some cases, are the position angles indicated in a catalog such as the UGC (Nilson 1973). Only two galaxies, UGC 477 and UGC 1281, had position angles well constrained by ROTCUR.

Ring radii were set to the effective fiber resolution for each galaxy. The resulting rotation curve was inspected for rings with considerably higher or lower velocities than neighboring rings. These highly deviant points in the rotation curve were investigated and were usually attributable to a single fiber in the ring having an extreme velocity. These extreme fibers were removed, and the rotation curve was recalculated. Finally, we added in quadrature to the error bars on the final rotation curve the velocity error from centroiding accuracy, corrected for inclination. We did not impose a minimum error on the rotation curve points, as was the case in some previous works (e.g., 5 km s^{-1} in Swaters et al. 2003a and 4 km s^{-1} in BMR01). The nature of the errors on the rotation curve points from the velocity fields is different from that of the errors on long-slit rotation curves. In the long-slit case, the error is on a single velocity measurement and gives the

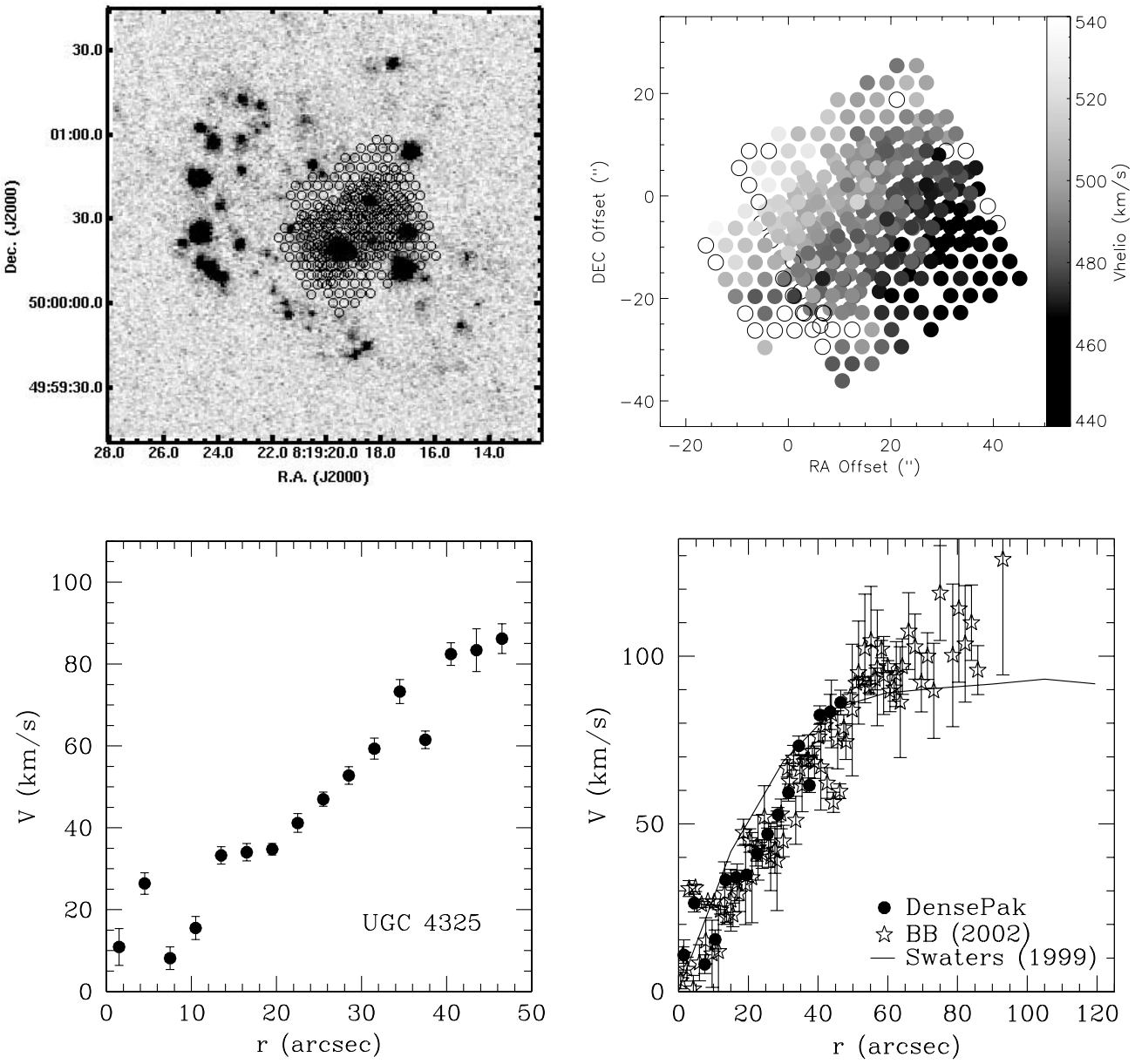

FIG. 1.—Results for UGC 4325. *Top left:* Position of DensePak array on the Hα image of the galaxy. This is an example of where interstitial pointings have been made to fill in the gaps between the fibers. *Top right:* Observed DensePak velocity field. Empty fibers are those without detections. *Bottom left:* DensePak rotation curve. *Bottom right:* DensePak rotation curve plotted with the raw long-slit Hα rotation curve of BB02 and the H I rotation curve of Swaters (1999). The H I data were excluded from the halo fits. [*See the electronic edition of the Supplement for a color version of this figure*.]

accuracy with which a Gaussian could be fitted to an emission-line profile, or the error is given by the consistency of the observed emission lines (Hα, [N II] λ6584, [S II] λ6717, and [S II] λ6731). The error does not contain information about the uncertainty in the rotation velocity. Errors can become arbitrarily small in high signal-to-noise ratio data, and this is why minimum errors were imposed. In two-dimensional data, the rotation velocity is obtained from a tilted-ring fit. The error indicates something about the spread of the velocities in a ring. In this case, a smaller error indicates that the gas in the ring has smaller noncircular motions.

4. RESULTS FOR INDIVIDUAL GALAXIES

In this section, we present the DensePak fiber positions, observed velocity fields, and rotation curves in Figures 1–11. A description is given for each galaxy, and we compare the rotation curves to previous raw long-slit Hα rotation curves, as well as H I rotation curves when available. Properties of the galaxies for which rotation curves are derived are listed in Table 1; there were 17 observed galaxies for which meaningful velocity fields could not be constructed.[4] As a result of remarkably poor weather, a number of galaxies have lopsided DensePak coverage.

UGC 4325.—This galaxy is large on the sky, and four DensePak pointings were made on the approaching side. The positions are shown on the Hα image from van Zee (2000). The fiber velocities were the average of the Hα and [S II] λ6717 lines. Hα is prevalent and was detected in almost every fiber. The position angle was fixed at the average of the position angles of previous long-slit observations (BB02; Swaters et al. 2003a). There is

[4] CamB, F750-4, KK98 251, UGC 891, UGC 1501/NGC 784, UGC 2455/NGC 1156, UGC 2864, UGC 4543, UGC 4787, UGC 5414/NGC 3104, UGC 7603/NGC 4455, UGC 8837/DDO 185, UGC 9211/DDO 189, UGC 11583, UGC 12344, UGC 12713, and UGC 12791.

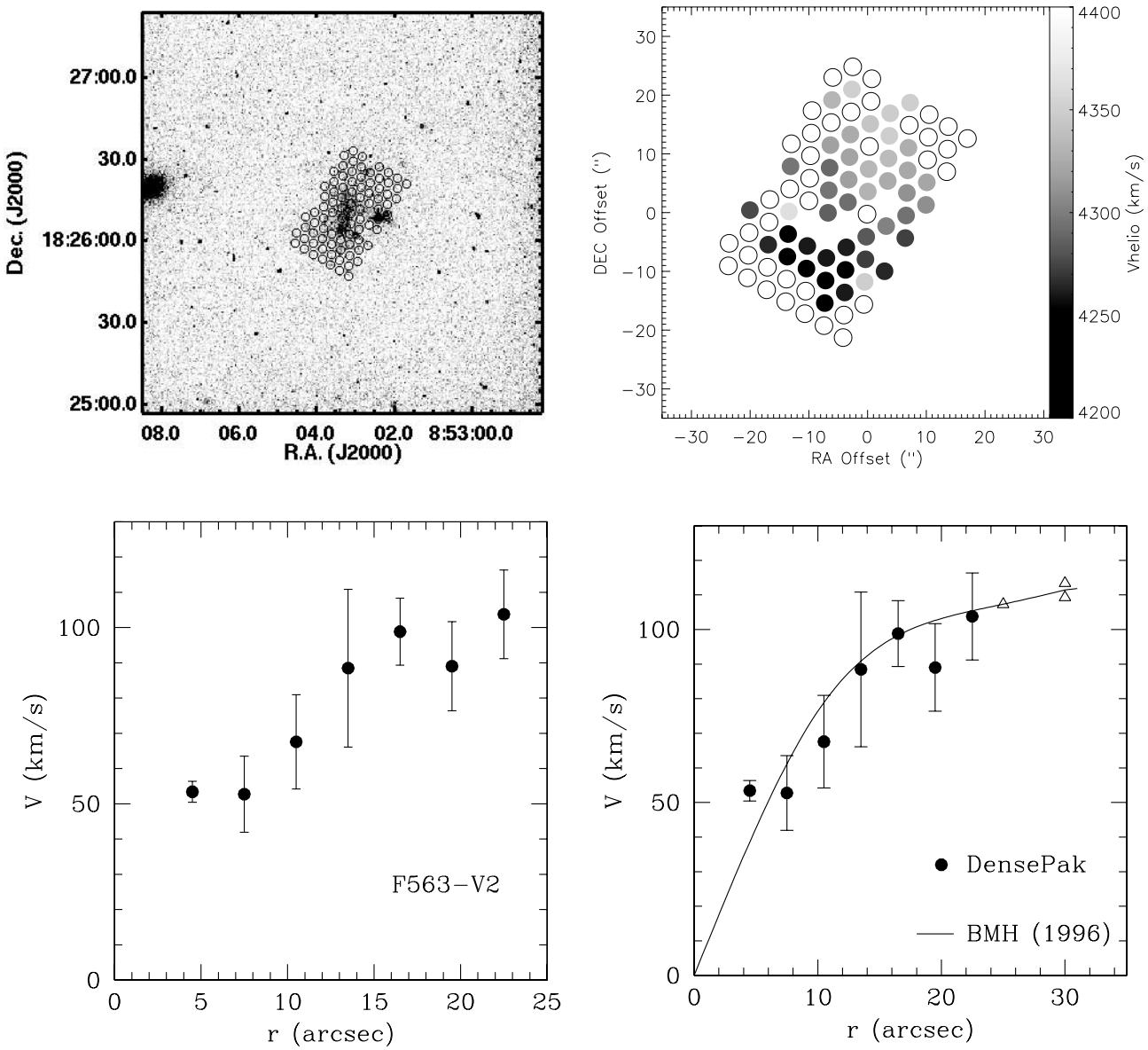

FIG. 2.—Results for F563-V2. *Top left:* Position of DensePak array on an Hα image of the galaxy. *Top right:* Observed DensePak velocity field. Empty fibers are those without detections. *Bottom left:* DensePak rotation curve. *Bottom right:* DensePak rotation curve plotted with the H I rotation curve of BMH96. Triangles represent the H I points used in the halo fits. [*See the electronic edition of the Supplement for a color version of this figure*.]

excellent agreement between the DensePak rotation curve and the long-slit Hα rotation curve of BB02. Very similar results have also been obtained with SparsePak (R. A. Swaters 2005, private communication). The H I data (Swaters 1999) lie above the optical data at the inner radii. This suggests that the H I data have been overcorrected for beam smearing (BB02). The outer H I points are a bit lower than the optical data but are within 1 σ. The decline in the rotation curve at the outer radii may be a real feature (Bosma 2004).

F563-V2.—There was one pointing for this galaxy. The DensePak fibers are shown on the Hα image from McGaugh et al. (1995). The fiber velocities were the average of the Hα, [S II] λ6717, and [S II] λ6731 lines. There is little Hα emission, and only roughly half of the fibers have an Hα detection. The position angle was fixed to the value used in Swaters et al. (2003a). The DensePak rotation curve generally agrees with the H I rotation curve of BMH96.

F563-1.—There was one pointing for this galaxy. The fiber positions are shown on an Hα image (W. J. G. de Blok 2005, unpublished data). The fiber velocities were the average of the Hα, [S II] λ6717, and [S II] λ6731 lines. The fibers were offset toward the receding side of the galaxy, and there was very little emission in the fibers on the approaching side. The position angle was fixed to the value in MRB01 and BB02. When compared to the long-slit Hα rotation curves of BMR01 and BB02, there is good agreement up to 15″. Beyond that, however, the long-slit curves and the H I curve (BMH96) turn over and flatten out, while the DensePak curve continues to rise. Additional DensePak coverage would be useful in determining where the DensePak curve turns over.

DDO 64.—There were three pointings for the center and approaching side of this galaxy. The DensePak fiber positions are shown on a Digitized Sky Survey[5] image. Fiber velocities were the average of the Hα and [S II] λ6717 lines. The amount of

[5] The Digitized Sky Surveys were produced at the Space Telescope Science Institute under NASA grant NAG W-2166. The images of these surveys are based on photographic data obtained using the Oschin Schmidt Telescope on Palomar Mountain and the UK Schmidt Telescope. The plates were processed into the present compressed digital form with the permission of these institutions.

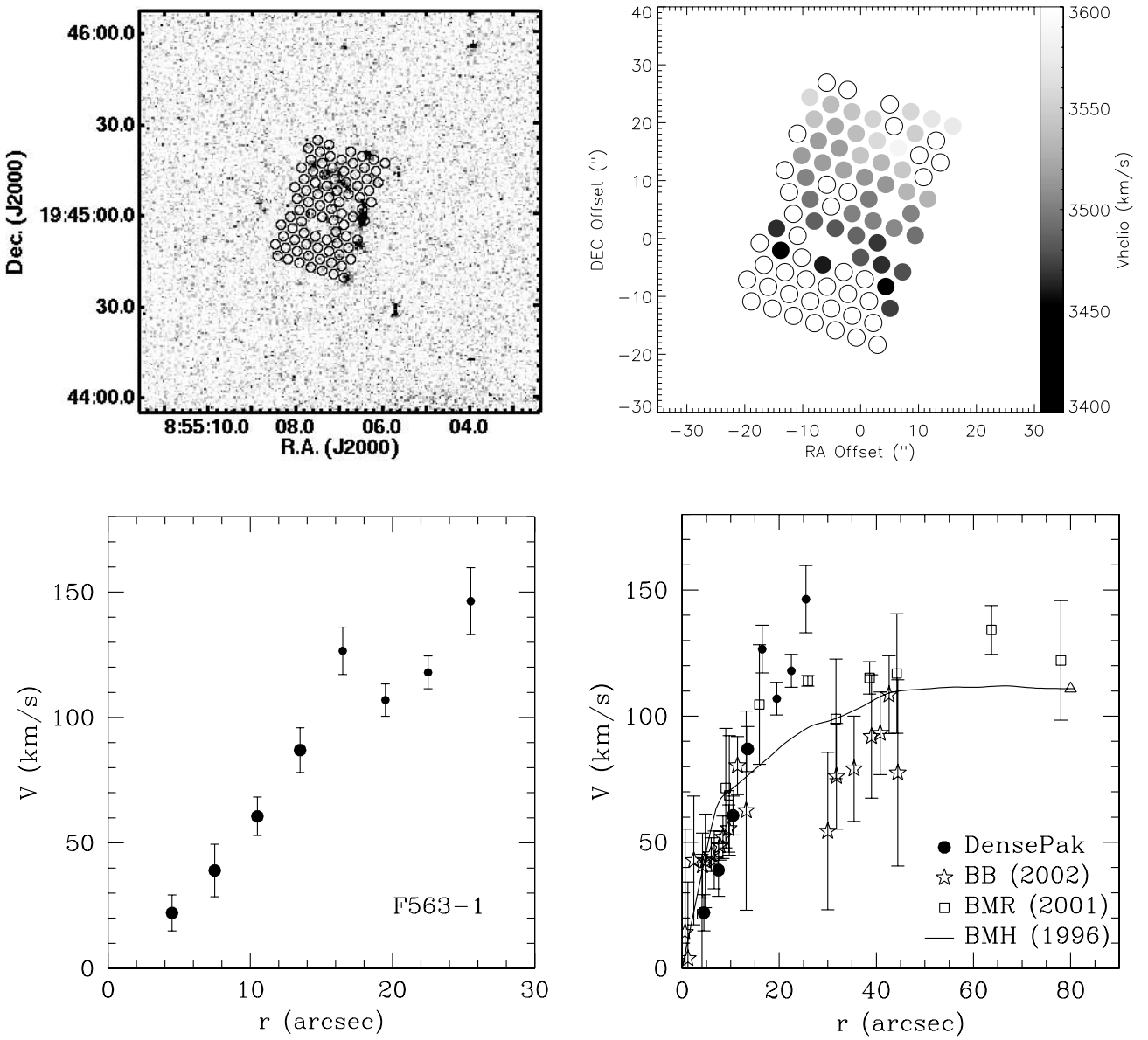

FIG. 3.—Results for F563-1. *Top left:* Position of DensePak array on an Hα image of the galaxy. *Top right:* Observed DensePak velocity field. Empty fibers are those without detections. *Bottom left:* DensePak rotation curve. The last four points are omitted from the halo fits. *Bottom right:* DensePak rotation curve plotted with the raw long-slit Hα rotation curves of BB02 and BMR01 and the H I rotation curve of BMH96. The triangle represents the H I point used in the halo fits. [*See the electronic edition of the Supplement for a color version of this figure.*]

emission in this galaxy is very high, and nearly all fibers detected emission. The position angle was fixed to the BB02 value. The DensePak points rise and fall in a pattern similar to the long-slit data (BB02). The structure in the rotation curve appears to be real. That the inner two points fall below the long-slit data may suggest the presence of noncircular motions in the inner regions. The H I data (Stil 1999) lie slightly below, but within the errors of, the optical data. It should be noted, however, that over the radial range plotted in Figure 4 there are only two H I points.

F568-3.—There was one pointing for this galaxy, and the fiber positions are shown on an Hα image (W. J. G. de Blok 2005, unpublished data). The fiber velocities were the average of the Hα and the [N II] λ6584 lines. Hα emission was detected in roughly 60% of the fibers. The position angle was fixed to the MRB01 and Swaters et al. (2003a) long-slit value. The DensePak rotation curve is consistent with the long-slit Hα curve of BMR01 and the H I curve of BMH96.

UGC 5750.—There was one pointing for this galaxy. The fiber positions are shown on an Hα image (W. J. G. de Blok 2005, unpublished data). The average of the Hα, [N II] λ6584, [S II] λ6717, and [S II] λ6731 lines was taken as the fiber velocity. Hα emission was sparse in this galaxy, and only roughly half of the fibers had a detection. The position angle was fixed to the value listed in MRB01 and BB02. There is good agreement with the long-slit Hα rotation curves of both BB02 and BMR01.

NGC 4395.—There were five pointings for this galaxy, and the positions of the DensePak fibers are shown on an *R*-band image (W. J. G. de Blok 2005, unpublished data). The Hα line overlapped slightly with a sky line. This was not a serious problem for this galaxy, because the emission lines (particularly the Hα line) were very strong. The Hα line was measured in a fiber if the [N II] λ6584, [S II] λ6717, and [S II] λ6731 lines were visible and strong and if the Hα line was stronger than the neighboring sky lines. With these criteria, Hα was detected in nearly all the fibers. The

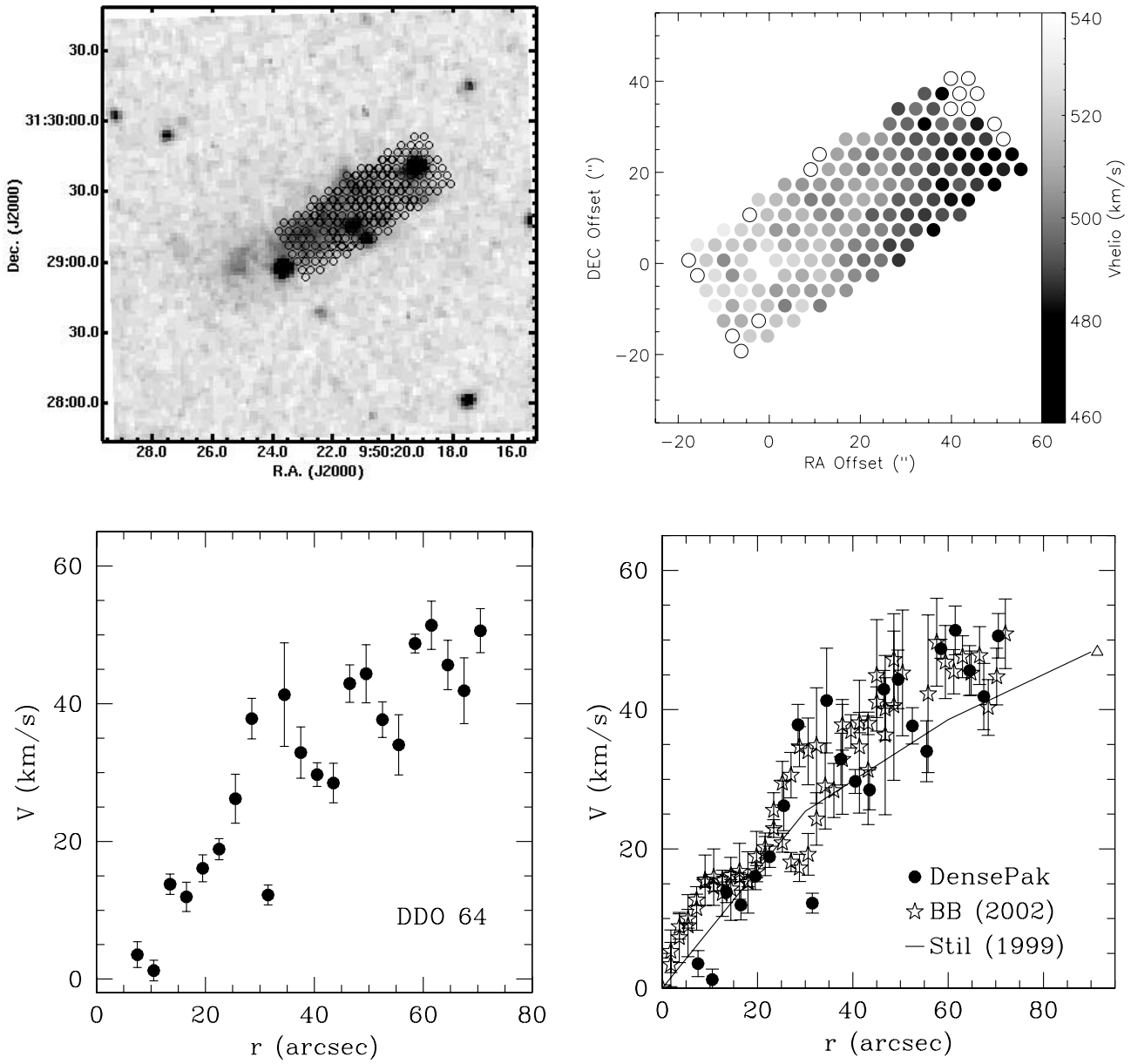

FIG. 4.—Results for DDO 64. *Top left:* Position of DensePak array on a Digitized Sky Survey image of the galaxy. *Top right:* Observed DensePak velocity field. The empty fibers are those without detections. *Bottom left:* DensePak rotation curve. *Bottom right:* DensePak rotation curve plotted with the raw long-slit Hα rotation curve of BB02 and the H I rotation curve of Stil (1999). The triangle represents the H I point used in the halo fits. [*See the electronic edition of the Supplement for a color version of this figure*.]

fiber velocities were the average of the Hα and [S II] λ6717 lines. The position angle of BB02 was used as the DensePak position angle. The DensePak rotation curve is consistent with the long-slit Hα curve of BB02, as well as the H I curve (Swaters 1999) at the innermost radii. At the outer radii, the H I curve falls below the optical data at about the 2 σ level.

F583-4.—There were two pointings for this galaxy: a central pointing and an interstitial pointing; the fiber positions are shown on the *R*-band image from BMH96. The fiber velocities are the averages of the Hα, [S II] λ6717, and [S II] λ6731 lines, and the approaching side of the galaxy has slightly better coverage than the receding side. The position angle was fixed to the value in MRB01. The DensePak rotation curve is generally consistent with the long-slit Hα rotation curve of BMR01. Both optical rotation curves are offset to noticeably higher velocities than the H I rotation curve of BMH96. This is one of the few galaxies where beam smearing in the H I data turned out to be important (BMR01).

F583-1.—There is one pointing for this galaxy. The DensePak fibers are shown on the *R*-band image of the galaxy from BMH96. The fiber velocities are the averages of the Hα, [S II] λ6717, and [S II] λ6731 lines, and more of the approaching side of the galaxy is seen than the receding side. The MRB01 position angle was taken as the DensePak position angle. The DensePak rotation curve is consistent with both the long-slit Hα rotation curve of BMR01 and the H I rotation curve of BMH96.

UGC 477.—There were three interstitial pointings along the length of this galaxy, and spatial coverage of the galaxy was optimal. The DensePak fibers are shown on the *R*-band image obtained at the KPNO 2 m telescope. Fiber velocities were the average of the Hα, [N II] λ6584, [S II] λ6717, and [S II] λ6731 lines. The amount of emission was very high in this galaxy, and

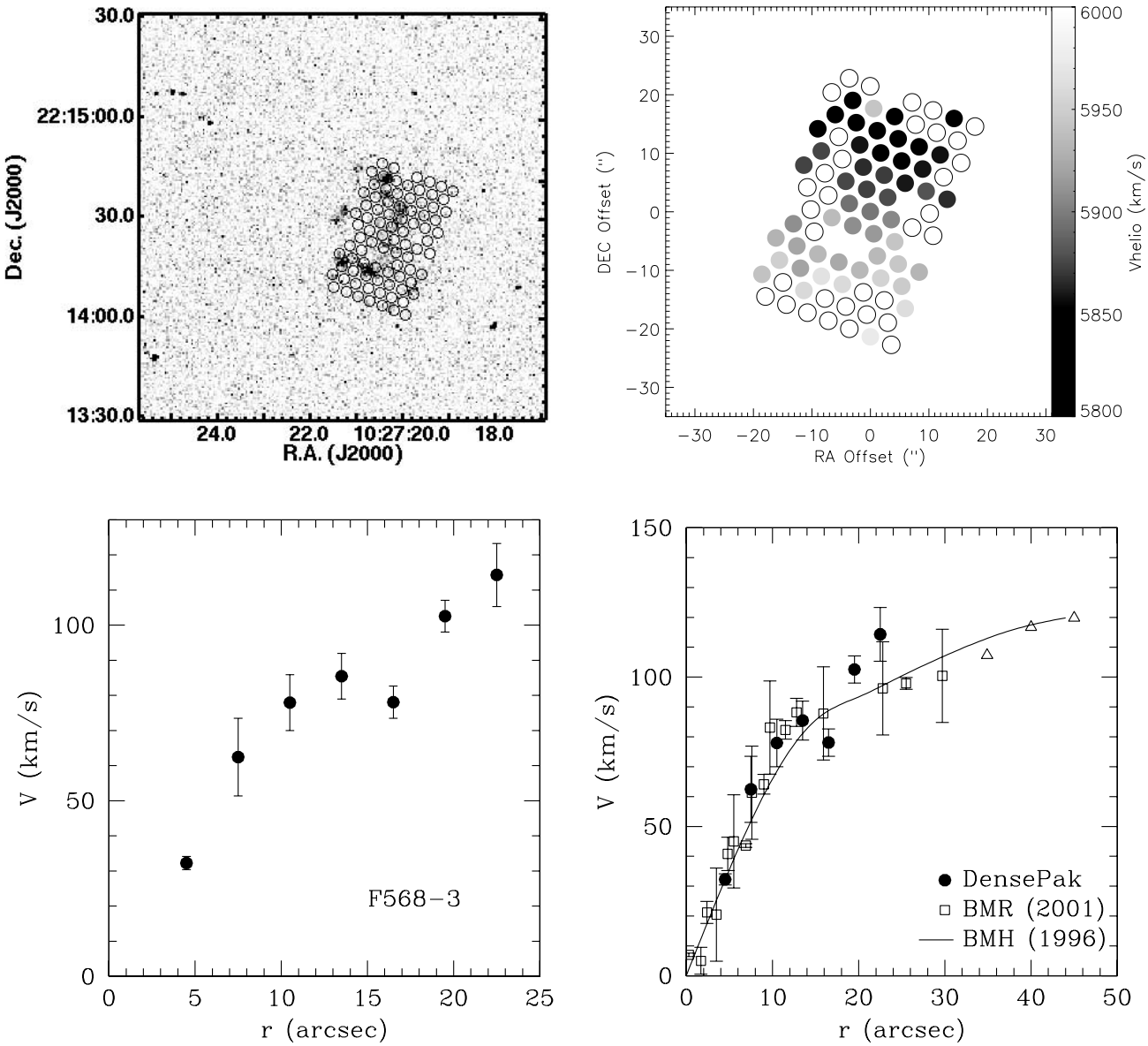

FIG. 5.—Results for F568-3. *Top left:* Position of DensePak array on an Hα image of the galaxy. *Top right:* Observed DensePak velocity field. The empty fibers are those without detections. *Bottom left:* DensePak rotation curve. *Bottom right:* DensePak rotation curve plotted with the raw long-slit Hα rotation curve of BMR01 and the H I rotation curve of BMH96. Triangles represent the H I points used in the halo fits. [*See the electronic edition of the Supplement for a color version of this figure*.]

almost every fiber had a detection. The position angle was well constrained by the data.

UGC 1281.—There were five interstitial pointings for this galaxy. The amount of emission was sparse, as fewer than 50% of the fibers had a detection. The DensePak fibers are shown on the *R*-band image obtained at the KPNO 2 m telescope. Fiber velocities were the average of the Hα, [S II] λ6717, and [S II] λ6731 lines. The position angle was well constrained by the data, and the DensePak rotation curve is consistent with the long-slit Hα rotation curve of BB02. UGC 1281 is a nearly edge-on galaxy. At high inclination, line-of-sight integration effects become important and may cause an intrinsically steeply rising rotation curve to appear slowly rising. The shape of the emission-line profiles can be used to constrain the shape of the rotation curve. If instrumental resolution is high enough and there is no line-of-sight obscuration, then symmetric line profiles indicate a solid-body rotation curve and skewed line profiles indicate a curved, NFW-like rotation curve (Kregel et al. 2004). The line profiles in the DensePak fibers are symmetric. UGC 1281 is unlikely to be so optically thick that the observations are hampered by obscuration (de Naray et al. 2004). Our instrumental resolution, however, is probably not high enough to resolve any skewing that may be present. We present the minimum-disk case analysis for this galaxy in § 5.2 but exclude it from further modeling.

Obtaining high-quality velocity fields is not trivial. LSB galaxies are difficult to observe. The Hα emission is faint. In addition, the emission may not be spread out enough to be detected across the entire DensePak fiber array. Although we tried to select galaxies with promising Hα emission, the remaining 17 galaxies of our sample[6] were observed, but unfortunately the detections were not good enough to construct meaningful velocity fields.

For the 11 galaxies for which we have constructed velocity fields, there is good overall agreement between the new DensePak rotation curves and the previous data sets. In all cases, the data are

[6] For a list of these galaxies, see footnote 4 in § 4.

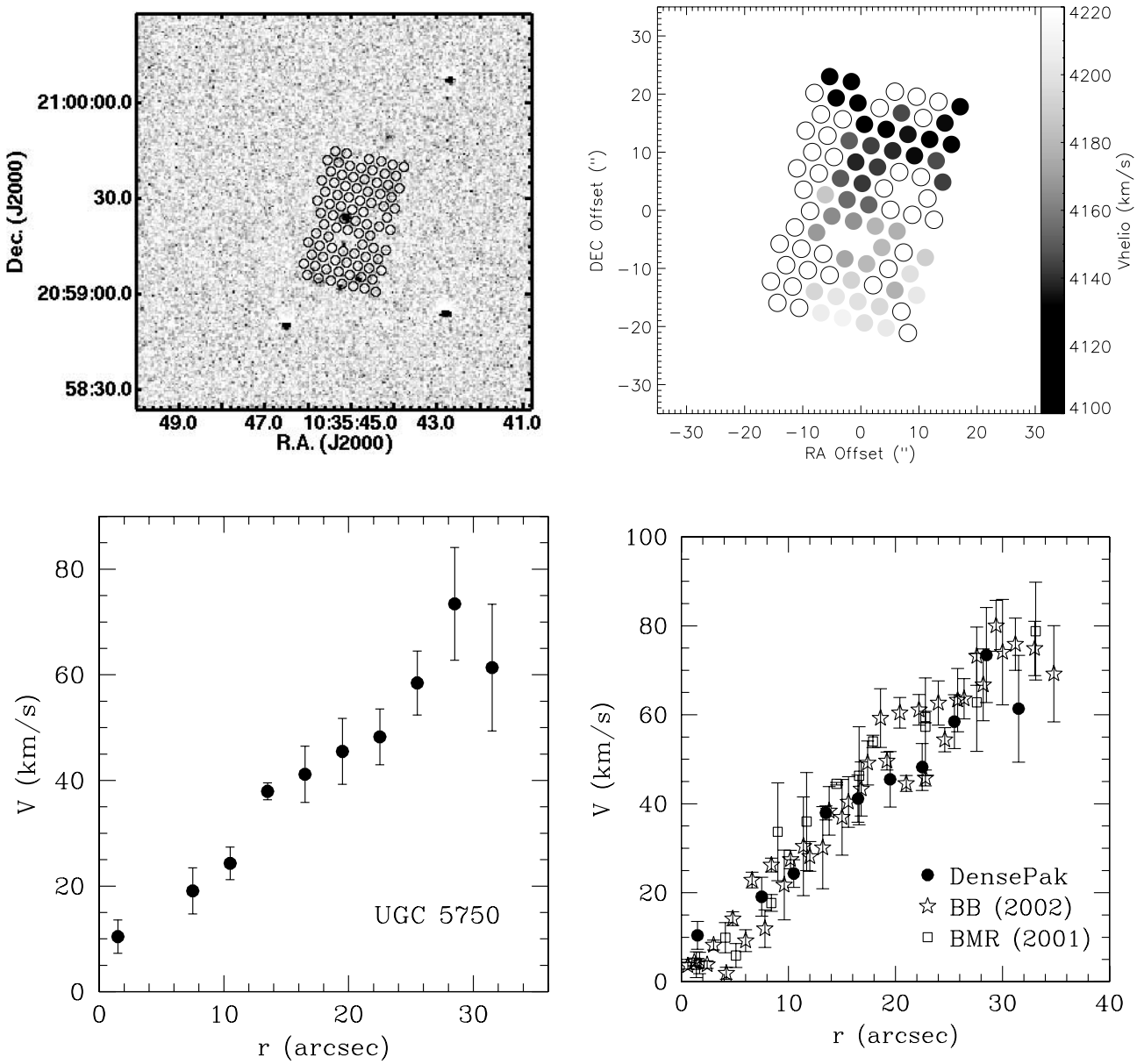

FIG. 6.—Results for UGC 5750. *Top left:* Position of DensePak array on an Hα image of the galaxy. *Top right:* Observed DensePak velocity field. Empty fibers are those without detections. *Bottom left:* DensePak rotation curve. *Bottom right:* DensePak rotation curve plotted with the raw long-slit Hα rotation curves of BB02 and BMR01. [*See the electronic edition of the Supplement for a color version of this figure.*]

broadly consistent with previous long-slit rotation curves. In only two cases, F563-1 and F583-4, do these independent data seem to differ, and then only over a very limited range in radius. In cases where H I data are available, five are in good overall agreement. In two cases, DDO 64 and F583-4, the H I data are somewhat lower than the optical data. In one case, UGC 4325, the H I data are too high. It is tempting to blame these cases on beam smearing or, in the case of UGC 4325, overcorrection for beam smearing, although other factors, such as the intrinsic H I distribution, are also relevant. On the whole, we are encouraged by the extent to which various independent data sets agree, given the difficult observational challenge posed by LSB galaxies.

5. PRELIMINARY ANALYSIS AND DISCUSSION

In this section, we wish to give an impression of how well the data are described by various halo models. We limit this discussion to the minimum-disk case in which we ignore the contribution of the stars and gas and attribute all rotation to dark matter. This puts an upper limit on the slope and/or concentration of the halo density profile. More detailed analysis, including mass modeling, will be presented in a future paper.

5.1. *Halo Models*

Two of the most prominent competing dark matter halo density profiles are the pseudoisothermal halo and the NFW profile. We provide a brief description of each below.

5.1.1. *Pseudoisothermal Halo*

The density profile of the pseudoisothermal halo is

$$\rho_{\rm iso}(R) = \rho_0[1 + (R/R_c)^2]^{-1}, \quad (4)$$

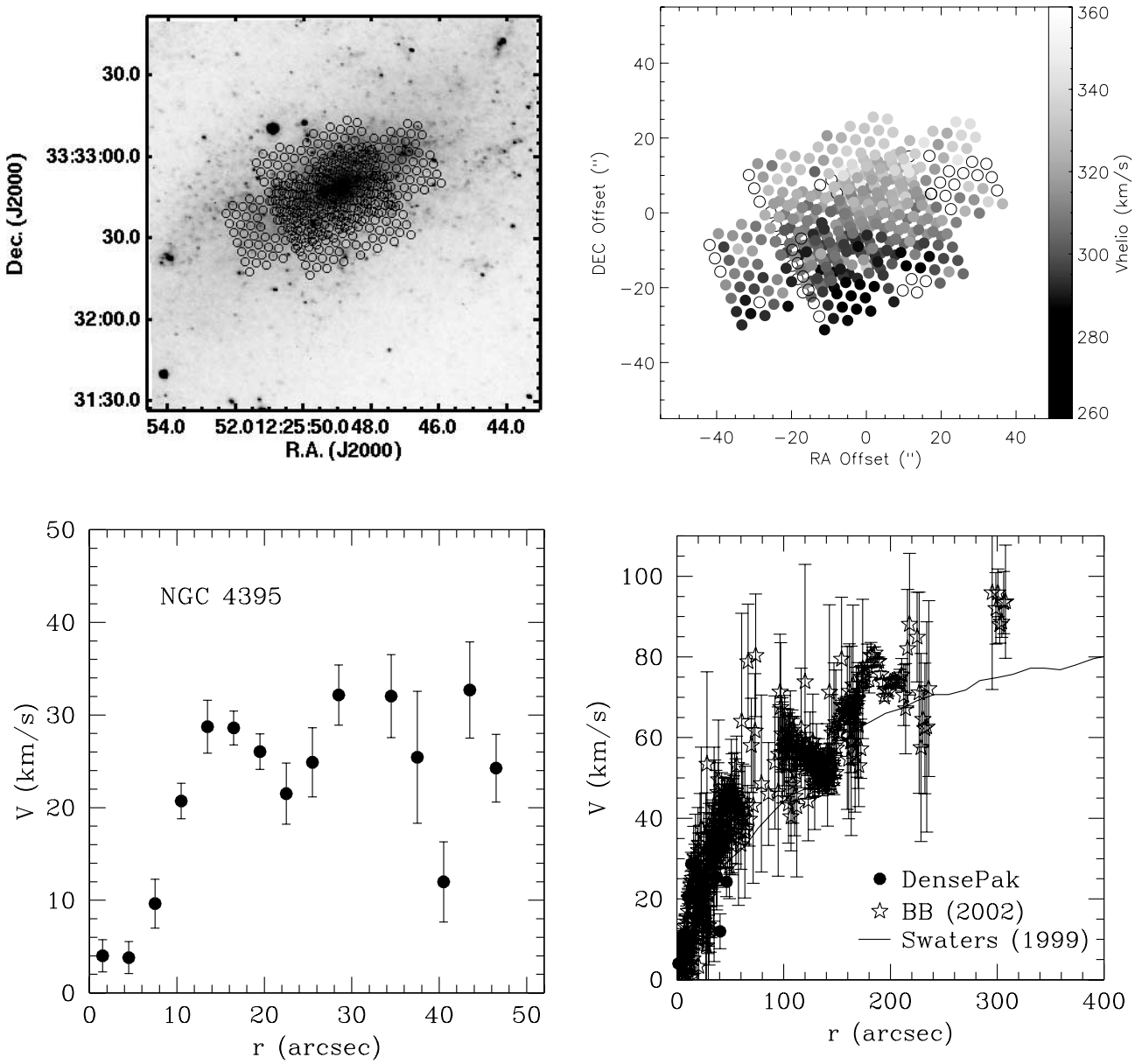

FIG. 7.—Results for NGC 4395. *Top left:* Position of DensePak array on an *R*-band image of the galaxy. *Top right:* Observed DensePak velocity field. Empty fibers are those without detections. *Bottom left:* DensePak rotation curve. *Bottom right:* DensePak rotation curve plotted with the raw long-slit Hα rotation curve of BB02 and the H I rotation curve of Swaters (1999). The H I points used in the halo fits extend beyond the radial range of this plot. [*See the electronic edition of the Supplement for a color version of this figure*.]

with ρ_0 being the central density of the halo and R_c representing the core radius of the halo. The rotation curve corresponding to this density profile is

$$V(R) = \sqrt{4\pi G\rho_0 R_c^2\left[1 - \frac{R_c}{R}\arctan\left(\frac{R}{R_c}\right)\right]}. \quad (5)$$

This form has traditionally been used in rotation curve fitting because it works well. By construction it produces flat rotation curves at large radii. This halo form is empirically motivated, predating those stemming from simulations.

5.1.2. *NFW Profile*

Numerical simulations produce the NFW profile and its variants. It predicts the same functional behavior for CDM halos of galaxy clusters as for the CDM halo of a single galaxy. The NFW mass density distribution is described as

$$\rho_{\rm NFW}(R) = \frac{\rho_i}{(R/R_s)(1 + R/R_s)^2}, \quad (6)$$

in which ρ_i is related to the density of the universe at the time of halo collapse and R_s is the characteristic radius of the halo. The NFW rotation curve is given by

$$V(R) = V_{200}\sqrt{\frac{\ln(1 + cx) - cx/(1 + cx)}{x[\ln(1 + c) - c/(1 + c)]}}, \quad (7)$$

with $x = R/R_{200}$. The rotation curve is parameterized by a radius R_{200} and a concentration parameter $c = R_{200}/R_s$, both of which are directly related to R_s and ρ_i. Here R_{200} is the radius at which the

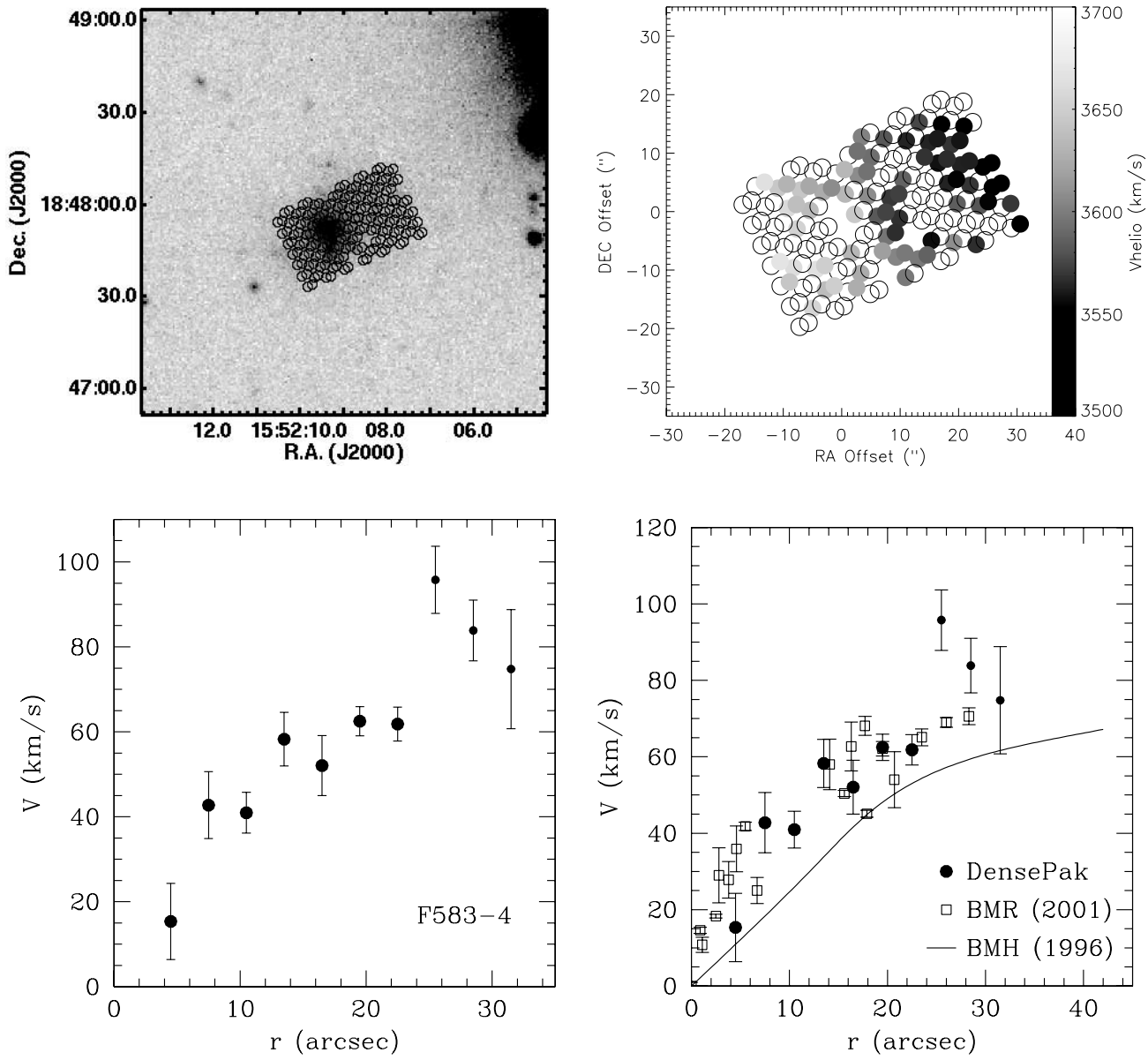

FIG. 8.—Results for F583-4. *Top left:* Position of DensePak array on an *R*-band image of the galaxy. *Top right:* Observed DensePak velocity field. Empty fibers are those without detections. *Bottom left:* DensePak rotation curve. The last three points were excluded from the halo fits. *Bottom right:* DensePak rotation curve plotted with the raw long-slit Hα rotation curve of BMR01 and the H I rotation curve of BMH96. The H I data were not included in the halo fits. [*See the electronic edition of the Supplement for a color version of this figure.*]

density contrast exceeds 200, roughly the virial radius; V_{200} is the circular velocity at R_{200} (Navarro et al. 1996). As mentioned in § 1, there are other cuspy halo models with slopes steeper than the NFW profile (e.g., Moore et al. 1999; Reed et al. 2003; Navarro et al. 2004; Diemand et al. 2005). The NFW profile thus serves as a lower limit to the slope of cuspy density profiles and, as such, gives the cuspy halo the best possible chance to fit the data. From an observational perspective, there is very little to distinguish the various flavors of cuspy halos.

5.2. *Halo Fits to Combined Data*

In this section, we combine the DensePak data with the previous smoothed long-slit Hα and H I rotation curves when available. For the 10 galaxies with long-slit and/or H I data, we supplement the DensePak data with the entire long-slit rotation curve and include only those H I points that extend beyond the radial range of both the DensePak and long-slit data. Using only the outer H I points, where the rotation curves have usually begun to flatten, lessens possible resolution effects. As discussed below, there are three galaxies, F563-1, F583-4, and UGC 4325, for which we exclude some of the DensePak and/or H I data.

We find the best-fit isothermal halo and NFW halo. This NFW halo fit is referred to as $\mathrm{NFW_{free}}$. The $\mathrm{NFW_{free}}$ halo fits do not necessarily have parameters that are realistic or consistent with ΛCDM. There is a tendency for the fits to drive toward very low c and very high V_{200}. There is also a c-V_{200} degeneracy that allows halos of different (c, V_{200}) to look the same over a finite range of radius. It is common for the $\mathrm{NFW_{free}}$ halos to overshoot the data at small radii, then undershoot the data, and then overshoot the data again and provide a poor description of the data at large radii. To address this, we also make a fit that we refer to as $\mathrm{NFW_{constrained}}$ (hereafter $\mathrm{NFW_{constr}}$). This halo was required to match the velocities at the outer radii of each galaxy while constraining the concentration to agree with cosmology. We chose a

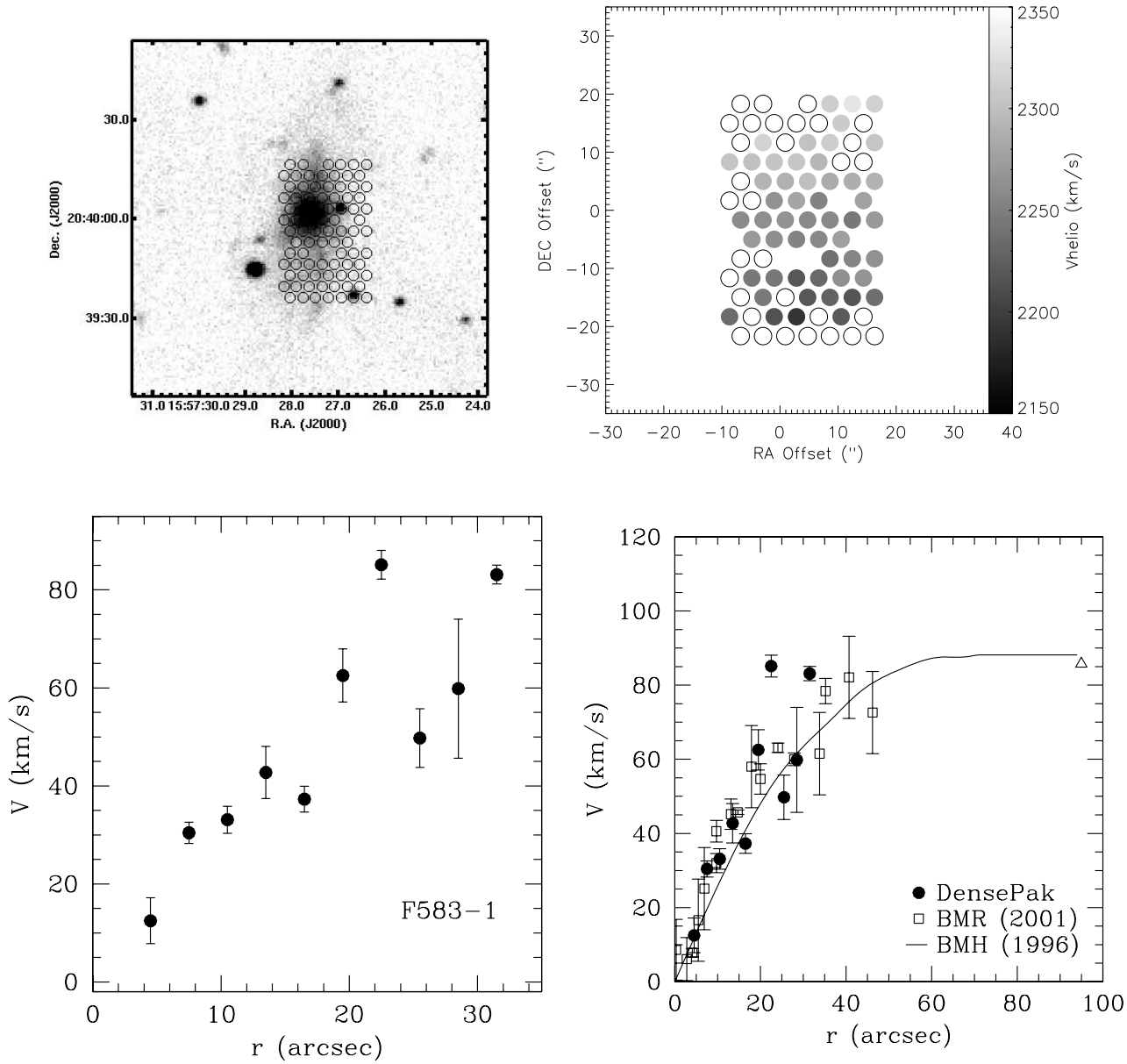

FIG. 9.—Results for F583-1. *Top left:* Position of DensePak array on an *R*-band image of the galaxy. *Top right:* Observed DensePak velocity field. Empty fibers are those without detections. *Bottom left:* DensePak rotation curve. *Bottom right:* DensePak rotation curve plotted with the raw long-slit Hα rotation curve of BMR01 and the H I rotation curve of BMH96. The triangle represents the H I point used in the halo fits. [*See the electronic edition of the Supplement for a color version of this figure*.]

value of V_{200} that forced the NFW velocities to match as many of the data points in the turnover region as closely as possible, with a minimum requirement of falling within the error bars. This is a reasonable constraint, because dark matter must explain the high velocities at large radii, where the contribution of the baryons has fallen off. Equation (7) of de Blok et al. (2003), which gives the concentration as a function of V_{200} (Navarro et al. 1997), was then used to calculate the concentration. We adjusted this concentration to agree with the cosmology of Tegmark et al. (2004) by subtracting 0.011 dex (McGaugh et al. 2003).

We did not include the last four DensePak points of F563-1 or the last three DensePak points of F583-4 in the halo fits. The F563-1 points were excluded because they are based on few fibers and because of the significant inconsistency with the long-slit and H I rotation curves, as discussed in § 4. The outer DensePak points of F583-4 spike to higher velocities than the long-slit data at the equivalent radii. Neither the isothermal nor the NFW halo model will be able to fit this feature in the DensePak rotation curve. These DensePak points also have little influence on the halo fits; there is essentially no change in the values of the isothermal or NFW halo parameters, but only much-improved χ^2, when the three DensePak points are removed. There are two and three H I points beyond the optical data for UGC 4325 and F583-4, respectively, that were also not used. Although the rise then sudden decline suggested by the combined optical and H I data for UGC 4325 may well be real, no simple, smooth model can fit it. Since we are interested in the inner halo structure as probed by the new data, we exclude the two H I points. For a thorough comparison of many more independent data for this galaxy, see Bosma (2004). The situation is similar for the H I points of F583-4.

In Figure 12, we plot the halo fits over the data, and we list the parameters in Table 2. We plot log V against log r to emphasize the fits to the data at small radii. The $\mathrm{NFW_{constr}}$ halos have already been required to match the data at large radii, and although

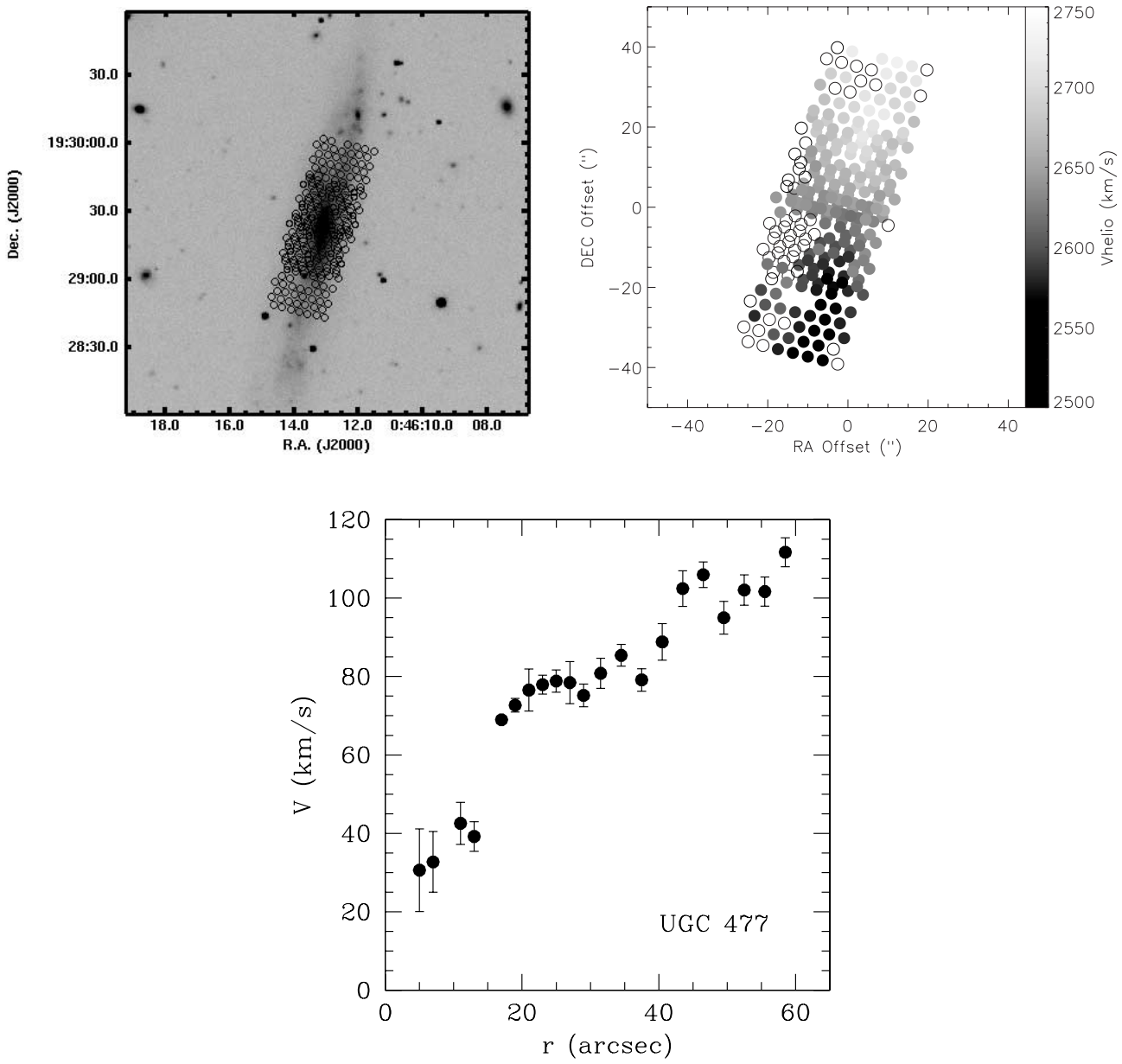

FIG. 10.—Results for UGC 477. *Top left:* Position of DensePak array on an *R*-band image of the galaxy. *Top right:* Observed DensePak velocity field. Empty fibers are those without detections. *Bottom:* DensePak rotation curve. [*See the electronic edition of the Supplement for a color version of this figure.*]

the best-fit NFW_{free} halos do not necessarily match the velocities at large radii, the magnitude of the discrepancy is generally smaller than it is at small radii.

No NFW_{free} fit could be made to four of the galaxies: UGC 4325, DDO 64, F568-3, and UGC 1281. Three galaxies, UGC 5750, F583-4, and F583-1, have concentrations too low to be consistent with ΛCDM. Specifically, the concentrations are farther from the concentrations of the NFW_{constr} halos than the expected log scatter in c of 0.18 (Bullock et al. 2001). Only the concentrations from the NFW_{free} fits of the remaining four galaxies, NGC 4395, UGC 477, F563-V2, and F563-1, are consistent with ΛCDM.

One should bear in mind that these fits are taken in the limit of minimum disk. Baryons do matter somewhat in LSB galaxies. This will drive the concentrations even lower in proper mass models.

The four galaxies for which no NFW_{free} fits could be made are fitted significantly better by isothermal halos than by NFW_{constr} halos. The case of F568-3 is typical: the NFW_{constr} halos overpredict the velocity at all radii interior to where they were forced to match the observed velocity. Of the galaxies with NFW_{free} fits, UGC 5750 is a good example of the over-under-over fitting trend of the NFW halo. This fitting trend has been observed before (e.g., BMR01; Gentile et al. 2004) and is what is being referred to when it is said that the NFW rotation curve has the wrong shape. Of the galaxies with NFW_{free} fits, UGC 5750, F583-1, and F563-1 are best fitted by isothermal halos in terms of χ_r^2. UGC 5750 is the strongest case, because the value of its best-fit concentration, 0.5, is far too low, according to current ideas from cosmological simulations. NGC 4395 has a reasonable NFW concentration and a χ_r^2 favoring the NFW halo. There are signs of a possible bar or oval structure at the center of this galaxy. Mass modeling beyond the minimum-disk case may help to determine the central structure of the galaxy and whether or not the NFW halo remains a good description of the data. F583-4 and F563-V2 also have χ_r^2 in favor of the NFW halo; however, the best-fit concentration for F583-4 is bordering on the low side of expected

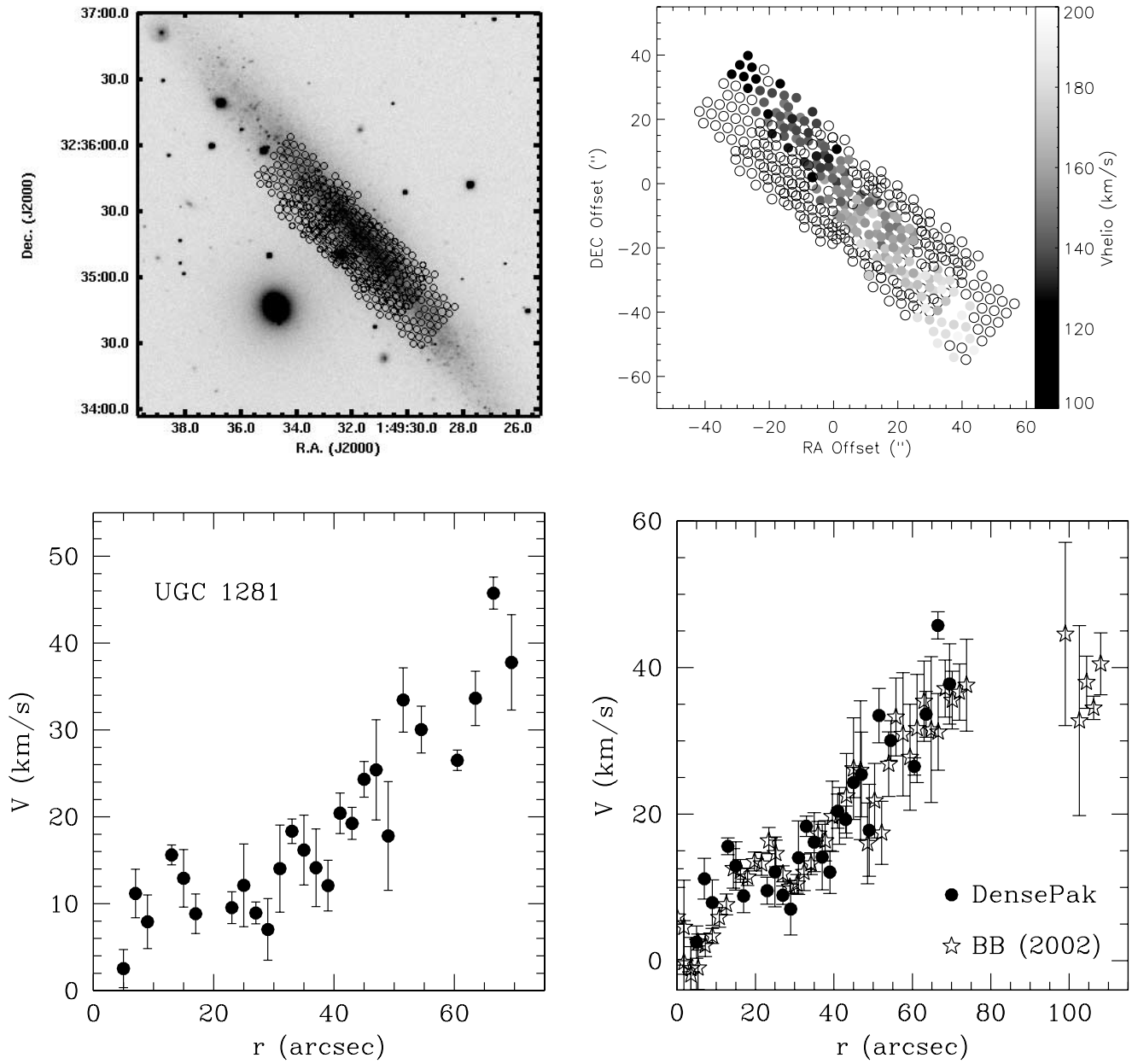

FIG. 11.—Results for UGC 1281. *Top left:* Position of DensePak array on an *R*-band image of the galaxy. *Top right:* Observed DensePak velocity field. Empty fibers are those without detections. *Bottom left:* DensePak rotation curve. *Bottom right:* DensePak rotation curve plotted with the raw long-slit Hα rotation curve of BB02. [*See the electronic edition of the Supplement for a color version of this figure.*]

values, and F563-V2 has too few data points to really distinguish between halo types. It is worth noting that when the small uncertainty in the first DensePak point of F563-V2 is increased to 5 km s^{-1}, neither the isothermal nor the NFW fit is significantly changed. Finally, UGC 477 is equally well fitted by both isothermal and NFW halos.

In total, seven galaxies are well described by the isothermal halo, one is consistent with NFW, and three are indistinguishable. For the majority of the galaxies, NFW halos either could not be fitted to the data or had concentrations too low to be consistent with ΛCDM. As shown by NGC 4395, velocities consistent with cuspy halos can be detected in the two-dimensional data.

5.3. *Comparison to Literature*

Ten of the 11 galaxies have published pseudoisothermal and NFW halo fits to the long-slit and/or H I data. In Figure 13, we plot the DensePak halo parameters for each galaxy (R_c and ρ_0 for isothermal, c and V_{200} for NFW) against the minimum-disk literature values. There is gross agreement between the DensePak and literature halo parameters, showing that the addition of the new two-dimensional optical data has not substantially altered the fits. The addition of the DensePak data does, however, bring down the errors on the halo parameters by roughly a factor of 2. The DensePak parameters are listed in Table 2; the numbers mentioned in the text below are from the cited references.

UGC 4325.—The DensePak isothermal halo parameters agree well with the results of BB02 ($R_c = 2.7 \pm 0.1$; $\rho_0 = 100.1 \pm 2.1$), and the agreement between those two data sets is better than the agreement of either set with the parameters of Swaters et al. (2003a; $R_c = 0.94$; $\rho_0 = 263$). No $\mathrm{NFW_{free}}$ fit could be made to the DensePak data, and the BB02 data preferred a concentration less than 0.1 ($c = 0.1$, $V_{200} = 3331.6$). Many of the BB02

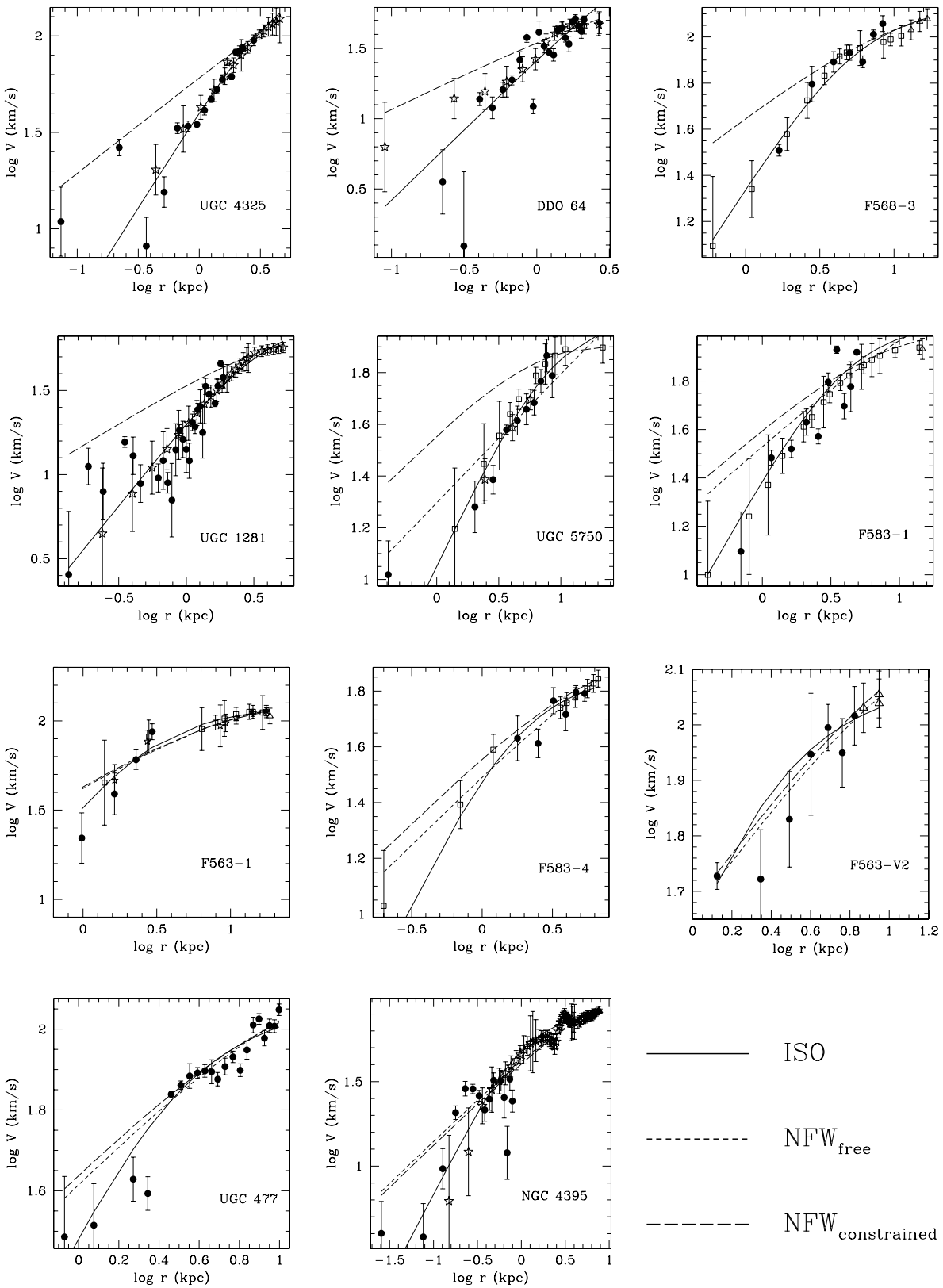

FIG. 12.—Halo fits to the combined DensePak and smoothed long-slit and H I rotation curves. Symbols areas in Figs. 1–11. The order of the galaxies has been changed from the order of Figs. 1–11 in order to show a progression in the halo fits. The fits change from isothermal to indistinguishable to NFW from top to bottom, left to right. [*See the electronic edition of the Supplement for a color version of this figure*.]

TABLE 2
BEST-FIT HALO PARAMETERS

	ISO			NFW_{free}			NFW_{constr}		
GALAXY	R_c (kpc)	ρ_0 ($10^{-3} M_\odot$ pc^{-3})	χ^2_r	c	V_{200} (km s^{-1})	χ^2_r	c	V_{200} (km s^{-1})	χ^2_r
UGC 4325	3.3 ± 0.2	91 ± 4	3.8	...	...	...	6.9	249	40
F563-V2	1.5 ± 0.1	119 ± 6	0.71	7.7 ± 2.0	128 ± 32	0.40	7.9	130	0.58
F563-1	2.1 ± 0.1	67 ± 2	0.43	7.8 ± 1.3	106 ± 10	0.88	8.4	101	0.95
DDO 64	4.4 ± 0.9	38 ± 3	5.5	...	...	...	9.2	62	20
F568-3	3.8 ± 0.2	27 ± 1	1.2	...	...	...	8.2	110	12
UGC 5750	5.7 ± 0.4	7.1 ± 0.3	0.83	0.5 ± 0.1	320 ± 43	1.7	9.1	67	25
NGC 4395	0.7 ± 0.1	258 ± 9	2.9	10.1 ± 0.6	77 ± 4	2.1	8.6	87	2.2
F583-4	1.3 ± 0.1	67 ± 2	0.67	5.5 ± 2.2	92 ± 32	0.41	9.1	67	1.1
F583-1	2.7 ± 0.1	35 ± 2	5.4	4.7 ± 0.7	133 ± 21	8.7	8.7	83	11
UGC 477	2.2 ± 0.1	57 ± 2	4.6	6.9 ± 0.6	120 ± 9	4.6	8.3	105	5.4
UGC 1281	2.6 ± 0.1	23 ± 1	3.8	...	...	...	9.3	58	25

NOTES.—Best-fit halo parameters for the combined DensePak, long-slit, and H I rotation curves.

galaxies have NFW fits with unphysical (very small or negative) values of the concentration. In these cases, the concentration was set to 0.1. The NFW fits by both Swaters et al. (2003a) and van den Bosch & Swaters (2001) required very high concentration values ($c = 14.8$, $V_{200} = 83$; $c = 30.9$, $V_{200} = 53.5$, respectively). The Swaters et al. (2003a) NFW fit shows the over-under-over fitting trend and is not a good representation of the data. For this galaxy, all of the listed concentrations are far beyond the reasonable range of expected values. The DensePak, BB02, and Swaters et al. (2003a) results all favor the isothermal halo as the best fit.

F563-V2.—For both the isothermal and NFW halo parameters, there is excellent agreement between the DensePak values and the results of the BMR01 analysis of the Swaters et al. (2000) data ($R_c = 1.69 \pm 0.17$, $\rho_0 = 131.2 \pm 19.4$). The error on each parameter has also been reduced by the DensePak data. The agreement is not as good with the isothermal parameters of Swaters et al. (2003a; $R_c = 1.13$; $\rho_0 = 231$). Their NFW concentration ($c = 14.4$) is again much higher than the DensePak value, and V_{200} much lower ($V_{200} = 92$). As previously discussed (see § 5.2), there are few points in the DensePak data, making a clear distinction between halo fits difficult. Certainly, there is nothing to contradict the conclusions of both previous studies that the data prefer the isothermal halo.

F563-1.—The DensePak results agree extremely well with both the isothermal ($R_c = 2.0 \pm 0.2$, $\rho_0 = 70.4 \pm 13.1$) and NFW ($c = 7.8 \pm 1.4$, $V_{200} = 106.8 \pm 10.3$) fits of BB02. The new data shrink the formal uncertainties on the isothermal halo parameters by a considerable amount. The level of agreement with the BMR01 results ($R_c = 1.72 \pm 0.23$, $\rho_0 = 91.9 \pm 21.6$; $c = 10.7 \pm 1.2$, $V_{200} = 93.1 \pm 4.3$) is only slightly less. The isothermal halo is preferred by all three studies.

DDO 64.—There is a difference between the isothermal halo parameters determined by the DensePak data and the results of BB02 ($R_c = 1.2 \pm 0.2$, $\rho_0 = 72.7 \pm 11.9$), but both studies prefer the isothermal halo to the NFW halo. The NFW results, however, are similar: no NFW_{free} fit could be made to the DensePak data, and the BB02 data favored a concentration less than 0.1 ($c = 0.1$, $V_{200} = 1182.3$). While the two isothermal fits are distinguishable, they are not too different. This galaxy seems to have real structure that is reflected in the rotation curve. The independent long-slit and DensePak data both show nonmonotonic features ("bumps and wiggles") that cannot be fitted by any simple, smooth halo models of the type considered here. There is more information in the data than a simple model can represent.

F568-3.—The isothermal halo parameters of the BMR01 analysis of the Swaters et al. (2000) data ($R_c = 3.93 \pm 0.75$, $\rho_0 = 30.2 \pm 5.6$) are in very good agreement with the DensePak results. Again, the DensePak parameters have lower errors. There is also moderate agreement between the DensePak parameters and the isothermal halo parameters of BMR01 ($R_c = 2.92 \pm 0.36$, $\rho_0 = 36.6 \pm 5.4$) and Swaters et al. (2003a; $R_c = 3.23$, $\rho_0 = 35.3$). No NFW_{free} fit could be made to the DensePak data, and all three other data sets require halos with low concentrations (BMR01 analysis of Swaters et al. 2000: $c = 1.2$, $V_{200} = 591.1$; BMR01: $c = 3.2 \pm 3.7$, $V_{200} = 214.6 \pm 233.9$; Swaters et al. 2003a: $c = 1.0$, $V_{200} = 637$). In all data sets, the isothermal halo is a better fit.

UGC 5750.—There is decent agreement with the DensePak isothermal halo parameters and the results of both BB02 ($R_c = 5.0 \pm 0.9$, $\rho_0 = 7.9 \pm 1.6$) and BMR01 ($R_c = 4.25 \pm 0.39$, $\rho_0 = 10.6 \pm 1.0$). The errors are lower on the DensePak-derived parameters. All three data sets require a very low NFW concentration (BB02: $c = 1.9 \pm 2.1$, $V_{200} = 145.7 \pm 122.9$; BMR01: $c = 2.6 \pm 1.5$, $V_{200} = 123.1 \pm 58.8$). The NFW halo is not a good description of the data. Although the formal fit parameters differ for the NFW halo, the degeneracy between halo parameters is such that there is little to distinguish the resulting halo rotation curve.

NGC 4395.—There is moderate agreement between the DensePak isothermal halo parameters and the values of the parameters found by BB02 ($R_c = 0.9 \pm 0.1$, $\rho_0 = 175.6 \pm 18.9$). The NFW_{free} concentration determined by the DensePak data is between the values listed in BB02 ($c = 12.1 \pm 0.9$, $V_{200} = 69.7 \pm 3.8$) and van den Bosch & Swaters (2001; $c = 8.5$, $V_{200} = 71.9$). As with UGC 5750, although the formal NFW fit parameters differ, the degeneracy between halo parameters is such that there is little to distinguish the resulting halo rotation curve. BB02 find the isothermal halo to be a slightly better fit to the data than the NFW halo, whereas the DensePak data have a slight preference for the NFW halo. The NFW halo certainly cannot be excluded, because it has a reasonable concentration in all three fits. The misalignment of the minor axis in the DensePak velocity field (see also Garrido et al. 2002; Noordermeer et al. 2001) and effects from star formation (BB02) need to be considered. The presence of a bar may create strong enough noncircular motions that the true potential is underestimated. Correcting for this would cause the halo profile to become more NFW-like. However, bars are disk dynamical features and imply that the disk has mass (which has so far been ignored in the

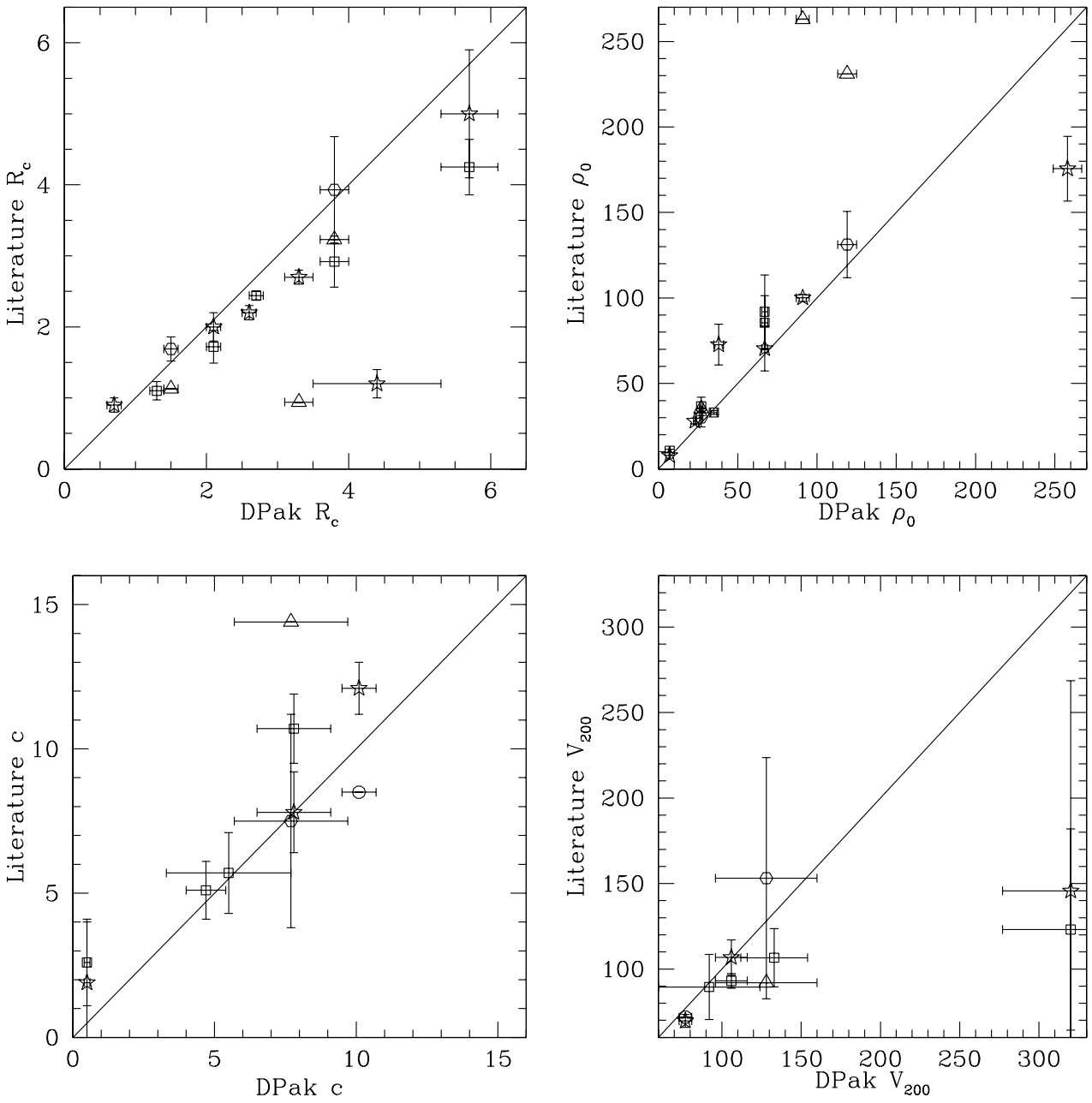

FIG. 13.—Comparison of DensePak halo parameters to previously published values. Values of R_c and ρ_0 are displayed for the isothermal halo, and c and V_{200} are shown for the NFW halo. Stars represent the data from BB02, squares the data from BMR01, triangles the data from Swaters et al. (2003a), circles the data from van den Bosch & Swaters (2001), and hexagons the BMR01 analysis of the Swaters et al. (2000) data. The addition of the DensePak does not significantly alter the previous halo fits but does reduce the errors on the halo parameters.

minimum-disk case) and would cause the halo profile to become more corelike.

F583-4.—The agreement between the DensePak halo parameters and the halo parameters of BMR01 is slightly better for the NFW halo ($c = 5.7 \pm 1.4$, $V_{200} = 89.5 \pm 19.0$) than for the isothermal halo ($R_c = 1.10 \pm 0.13$, $\rho_0 = 85.5 \pm 15.8$). Both data sets find the NFW halo to be a slightly better fit to the data.

F583-1.—There is good agreement of the isothermal ($R_c = 2.44 \pm 0.06$, $\rho_0 = 33.0 \pm 1.1$) and NFW ($c = 5.1 \pm 1.0$, $V_{200} = 106.6 \pm 17.0$) halo parameters of BMR01 with the DensePak parameters. Both data sets find the isothermal halo to be the better description of the data.

UGC 1281.—There is moderate agreement between the isothermal halo parameters of the DensePak data and the results of BB02 ($R_c = 2.2 \pm 0.1$, $\rho_0 = 28.0 \pm 1.7$). No $\mathrm{NFW_{free}}$ halo could be fitted to the DensePak data. The BB02 data required a very low concentration ($c = 0.1$, $V_{200} = 785$).

5.4. *A Word about Noncircular Motions*

The presence of noncircular motions may cause the circular velocity to be underestimated or, sometimes, overestimated (Swaters et al. 2003a). This effect has been suggested as a reason why cored halos appear to be preferred to those with cusps (e.g., Swaters et al. 2003a; van den Bosch & Swaters 2001). The presence of noncircular motions and the magnitude of the effect on the system can be qualitatively ascertained by looking at the velocity field. For instance, the alignment of the major and minor axes will begin to deviate from perpendicular (a mild example being NGC 4395). Or the isovelocity contours will become noticeably more kinked, wiggly, or twisted as noncircular motions increase. There are

TABLE 3
Galaxy Velocity Dispersions

Galaxy	Velocity Dispersion (km s^{-1})
UGC 4325	7.8
F563-V2	8.2
F563-1	8.1
DDO 64	6.2
F568-3	8.7
UGC 5750	8.7
NGC 4395	9.7
F583-4	9.5
F583-1	7.3
UGC 477	8.1
UGC 1281	6.9

Notes.—Velocity dispersion in the DensePak data for each galaxy. Values are between 6 and 10 km s^{-1} and are consistent with the typical dispersions for the gas components of galaxies.

indications of noncircular motions in some of our sample of galaxies, but how significant are they?

One way of measuring this is to look at the velocity dispersion about the mean difference of the individual fiber velocities from the circular velocity. The velocity dispersions measured in this fashion for each galaxy are listed in Table 3. The velocity dispersions are all in the range of 6–10 km s^{-1}. These values are totally consistent with the typical dispersions for the gas component of galaxies and suggest that we are not seeing signs of extreme noncircular motions. If added in quadrature to the rotation velocity, dispersions of this magnitude affect only the innermost points, where the rotation velocity and velocity dispersion are comparable. We tried this exercise assuming an isotropic dispersion ($v_{\rm circ}^2 = v_{\rm rot}^2 + 3\sigma^2$) for the UGC 5750 DensePak data. We chose UGC 5750 because, of the galaxies with NFW fits, it is the least consistent with the NFW halo and because it has the largest differences between the halo fits at low radii. With the exception of only the first data point, all corrected velocities remain within the errors of the uncorrected velocities. The first data point increases by $\sim$8 km s^{-1}, but this does not improve the NFW$_{\rm free}$ fit: the concentration remains virtually unchanged ($c = 0.4 \pm 0.1$). A more in-depth analysis of noncircular motions will be discussed in a future paper, but this simple analysis already suggests that the magnitude of realistic noncircular motions is not likely to be sufficient to recover the high-concentration cuspy halos expected from ΛCDM structure formation simulations.

6. CONCLUSIONS AND FUTURE WORK

We have presented the two-dimensional velocity fields and rotation curves of a sample of LSB galaxies that have been observed with DensePak. The majority of these new data have been shown to be consistent with the rotation curves of previous long-slit Hα and H I observations. In a preliminary analysis, we have combined these data and have fitted the minimum-disk case for three halo models: the best-fit isothermal halo, the NFW$_{\rm free}$ halo with no constraints on the parameters, and the NFW$_{\rm constr}$ halo, which was constructed to agree with ΛCDM cosmology. We found seven galaxies to prefer the isothermal halo, one to prefer the NFW halo, and three to show no clear preference. When NFW$_{\rm free}$ fits could be made, the concentrations were often too low, compared to the expected values for ΛCDM.

We have compared our DensePak halo fits to the results of previous studies. The DensePak halo parameters change little but do have improved uncertainties. Future work will include a detailed assessment of noncircular motions, slit placement, and mass modeling to determine the distribution of dark matter in more realistic cases than the minimum-disk scenario.

We would like to thank the referee for helpful comments. The work of R. K. d. N. and S. S. M. was supported by NSF grant AST 05-05956. This research has made use of the NASA/IPAC Extragalactic Database (NED), which is operated by the Jet Propulsion Laboratory, California Institute of Technology, under contract with the National Aeronautics and Space Administration. Our velocity field plots were made using a modified version of the program found at http://www.astro.wisc.edu/~mab/research/densepak/DP/dpidl.html.

REFERENCES

Begeman, K. G. 1989, A&A, 223, 47
Blais-Ouellette, S., Amram, P., & Carignan, C. 2001, AJ, 121, 1952
Bolatto, A. D., Simon, J. D., Leroy, A., & Blitz, L. 2002, ApJ, 565, 238
Borriello, A., & Salucci, P. 2001, MNRAS, 323, 285
Bosma, A. 2004, in IAU Symp. 220, Dark Matter in Galaxies, ed. S. D. Ryder, D. J. Pisano, M. A. Walker, & K. C. Freeman (San Francisco: ASP), 39
Bullock, J. S., Kolatt, T. S., Sigad, Y., Somerville, R. S., Kravtsov, A. V., Klypin, A. A., Primack, J. R., & Dekel, A. 2001, MNRAS, 321, 559
Côté, S., Carignan, C., & Freeman, K. C. 2000, AJ, 120, 3027
de Blok, W. J. G. 2004, in IAU Symp. 220, Dark Matter in Galaxies, ed. S. D. Ryder, D. J. Pisano, M. A. Walker, & K. C. Freeman (San Francisco: ASP), 69
de Blok, W. J. G., & Bosma, A. 2002, A&A, 385, 816 (BB02)
de Blok, W. J. G., Bosma, A., & McGaugh, S. 2003, MNRAS, 340, 657
de Blok, W. J. G., & McGaugh, S. S. 1996, ApJ, 469, L89
———. 1997, MNRAS, 290, 533
de Blok, W. J. G., McGaugh, S. S., Bosma, A., & Rubin, V. C. 2001a, ApJ, 552, L23
de Blok, W. J. G., McGaugh, S. S., & Rubin, V. C. 2001b, AJ, 122, 2396 (BMR01)
de Blok, W. J. G., McGaugh, S. S., & van der Hulst, J. M. 1996, MNRAS, 283, 18 (BMH96)
de Naray, R. K., McGaugh, S. S., & de Blok, W. J. G. 2004, MNRAS, 355, 887
Diemand, J., Zemp, M., Moore, B., Stadel, J., & Carollo, M. 2005, MNRAS, 364, 665
Flores, R. A., & Primack, J. R. 1994, ApJ, 427, L1
Fuchs, B. 2003, Ap&SS, 284, 719
Garrido, O., Marcelin, M., Amram, P., & Boulesteix, J. 2002, A&A, 387, 821
Gentile, G., Salucci, P., Klein, U., Vergani, D., & Kalberla, P. 2004, MNRAS, 351, 903
Kregel, M., van der Kruit, P. C., & Freeman, K. C. 2004, MNRAS, 351, 1247
Marchesini, D., D'Onghia, E., Chincarini, G., Firmani, C., Conconi, P., Molinari, E., & Zacchei, A. 2002, ApJ, 575, 801
McGaugh, S. S., Barker, M. K., & de Blok, W. J. G. 2003, ApJ, 584, 566
McGaugh, S. S., Rubin, V. C., & de Blok, W. J. G. 2001, AJ, 122, 2381 (MRB01)
McGaugh, S. S., Schombert, J. M., & Bothun, G. D. 1995, AJ, 109, 2019
Moore, B. 1994, Nature, 370, 629
Moore, B., Quinn, T., Governato, F., Stadel, J., & Lake, G. 1999, MNRAS, 310, 1147
Navarro, J. F., Frenk, C. S., & White, S. D. M. 1996, ApJ, 462, 563
———. 1997, ApJ, 490, 493
Navarro, J. F., et al. 2004, MNRAS, 349, 1039
Nilson, P. 1973, Uppsala General Catalogue of Galaxies (Uppsala Astron. Obs. Ann., Vol. 6)
Noordermeer, E., Sparke, L. S., & Levine, S. E. 2001, MNRAS, 328, 1064
Osterbrock, D. E., Fulbright, J. P., Martel, A. R., Keane, M. J., Trager, S. C., & Basri, G. 1996, PASP, 108, 277
Pickering, T. E., Impey, C. D., van Gorkom, J. H., & Bothun, G. D. 1997, AJ, 114, 1858
Pickering, T. E., van Gorkom, J. H., Impey, C. D., & Quillen, A. C. 1999, AJ, 118, 765

Reed, D., Gardner, J., Quinn, T., Stadel, J., Fardal, M., Lake, G., & Governato, F. 2003, MNRAS, 346, 565
Rhee, G., Valenzuela, O., Klypin, A., Holtzman, J., & Moorthy, B. 2004, ApJ, 617, 1059
Simon, J. D., Bolatto, A. D., Leroy, A., & Blitz, L. 2003, ApJ, 596, 957
Simon, J. D., Bolatto, A. D., Leroy, A., Blitz, L., & Gates, E. L. 2005, ApJ, 621, 757
Spekkens, K., Giovanelli, R., & Haynes, M. P. 2005, AJ, 129, 2119
Stil, J. 1999, Ph.D. thesis, Univ. Leiden
Swaters, R. A. 1999, Ph.D. thesis, Univ. Groningen
Swaters, R. A., Madore, B. F., & Trewhella, M. 2000, ApJ, 531, L107
Swaters, R. A., Madore, B. F., van den Bosch, F. C., & Balcells, M. 2003a, ApJ, 583, 732
Swaters, R. A., Verheijen, M. A. W., Bershady, M. A., & Andersen, D. R. 2003b, ApJ, 587, L19
Tegmark, M., et al. 2004, Phys. Rev. D, 69, 103501
Teuben, P. J. 1995, in ASP Conf. Ser. 77, Astronomical Data Analysis Software and Systems IV, ed. R. Shaw, H. E. Payne, & J. J. E. Hayes (San Francisco: ASP), 398
Tully, R. B. 1988, Nearby Galaxies Catalogue (Cambridge: Cambridge Univ. Press)
van den Bosch, F. C., Robertson, B. E., Dalcanton, J. J., & de Blok, W. J. G. 2000, AJ, 119, 1579
van den Bosch, F. C., & Swaters, R. A. 2001, MNRAS, 325, 1017
van Zee, L. 2000, AJ, 119, 2757